Evaluating the performance of the Canadian Land Surface Scheme Including Biogeochemical Cycles (CLASSIC) tailored to the pan-Canadian domain

Salvatore R. Curasi[1,2,https://orcid.org/0000-0002-4534-3344], Joe R. Melton[1,https://orcid.org/0000-0002-9414-064X], Elyn R. Humphreys[2,https://orcid.org/0000-0002-5397-2802], Libo Wang[3,https://orcid.org/0000-0002-3751-3390], Christian Seiler[1,https://orcid.org/0000-0002-2092-0168], Alex J. Cannon[1,https://orcid.org/0000-0002-8025-3790], Ed Chan[3,https://orcid.org/0000-0003-1160-1090], Bo Qu[4]

[1]Climate Research Division, Environment, and Climate Change Canada, Victoria, BC;
[2]Department of Geography & Environmental Studies, Carleton University, Ottawa, ON;
[3]Climate Research Division, Environment, and Climate Change Canada, Toronto, ON;
[4]Département de géographie, Université de Montréal, Montréal, QC, Canada

Key points:

- Using region-specific prescribed vegetation cover and adding five region-specific PFTs reduced model biases against reference data.
- CLASSIC's performance when tailored to the Canada domain is similar to that for comparisons between independent reference data sets.
- Future work should focus on boreal disturbance (i.e. fire, insect damage, and harvest), peatlands, and permafrost in Canada and other boreal regions.

Abstract:

Canada's boreal forests and tundra ecosystems are responding to unprecedented climate change with implications for the global carbon (C) cycle and global climate. However, our ability to model the response of Canada's terrestrial ecosystems to climate change is limited and there has been no comprehensive, process-based assessment of Canada's terrestrial C cycle. We tailor the Canadian Land Surface Scheme Including Biogeochemical Cycles (CLASSIC) to Canada and evaluate its C cycling performance against independent reference data. We utilize skill scores to assess model performance against reference data alongside benchmark scores that quantify the level of agreement between the reference data sets to aid in interpretation. Our results demonstrate CLASSIC's sensitivity to prescribed vegetation cover. They also show that the addition of five region-specific PFTs improves CLASSIC's skill at simulating the Canadian C cycle. CLASSIC performs well when tailored to Canada, falls within the range of the reference data sets, and meets or exceeds the benchmark scores for most C cycling processes. New region-specific land cover products, well-informed plant functional type (PFT) parameterizations, and more detailed reference data sets will facilitate improvements to the representation of the terrestrial C cycle in regional and global land surface models (LSMs). Incorporating a parameterization for boreal disturbance processes and explicitly representing peatlands and permafrost soils will improve CLASSIC's future performance in Canada and other boreal regions. This is an important step toward a comprehensive process-based assessment of Canada's terrestrial C cycle and evaluating Canada's net C balance under climate change.

Plain language summary:

Canada plays an important role in the global carbon cycle. Its boreal forests and tundra are responding to climate change. There has not been a comprehensive modeling assessment of Canada's land carbon cycle. We modify our model to better represent the distribution of plants in Canada and to include five new plant-type representations. We then compare results from our model and other independent observation-based data sets. Our modifications produced model results that agreed better with the independent data sets. This is an important step towards a comprehensive modeling assessment of Canada's land carbon cycle.

Keywords: Canada, boreal, Arctic, carbon cycle, land surface model, CLASSIC

1. Introduction

Canada's extensive boreal forests and tundra ecosystems are critical components of the global carbon (C) cycle (Keenan & Williams, 2018; Lenton et al., 2008; Miner et al., 2022; Myers-Smith et al., 2020; Qiu et al., 2020). Approximately 31% of the world's boreal forests and 36% of arctic tundra lie within Canada (Potapov et al., 2008; Walker et al., 2005). These ecosystems are responding to unprecedented climate change and anthropogenic activities with implications

for the region's C balance and global climate (Lenton et al., 2008; Myers-Smith et al., 2020; Schuur & Mack, 2018; White et al., 2017). Unfortunately, there has been no comprehensive, process-based assessment of Canada's terrestrial C cycle (Chaste et al., 2017; Friedlingstein et al., 2019; Peng et al., 2014). Moreover, our ability to investigate the response of Canada's terrestrial ecosystems to climate change is limited by the level of detail with which vegetation in Canada's boreal and tundra ecosystems is represented within models (D'Orangeville et al., 2018; Girardin et al., 2016; Marchand et al., 2018; Ma et al., 2012; Sulla-Menashe et al., 2018). Improving our ability to model Canada's terrestrial ecosystems will provide more accurate insight into Canada's historical and future C cycle while informing the implementation of the 2015 Paris Agreement (UNFCCC, 2015) and the Pan-Canadian Framework on Clean Growth and Climate Change (Government of Canada, 2016). A comprehensive process-based assessment of Canada's terrestrial C cycle could also be used to estimate emissions from the land sector in synergy with other efforts (e.g. Kurz et al., (2009)). Here we tailor the Canadian Land Surface Scheme Including Biogeochemical Cycles (CLASSIC) to the pan-Canadian domain (i.e. all of Canada south of 76° North) and evaluate its ability to represent the Canadian C cycle.

Boreal forests are responding to climate change, rising atmospheric CO_2 concentrations, water stress, permafrost thaw, and changing disturbance regimes (Babst et al., 2019; Potapov et al., 2008; Reich et al., 2018, 2022; Sulla-Menashe et al., 2018). Warmer temperatures and higher atmospheric CO_2 concentrations may increase the productivity of boreal forests (Ju & Chen, 2008; Sulla-Menashe et al., 2018). In contrast, increased drought stress and changing disturbance regimes may act to decrease boreal productivity and lead to the release of C from vegetation and soil (Babst et al., 2019; Lenton et al., 2008; Potapov et al., 2008; Reich et al., 2018; Weber & Flannigan, 1997). Not all boreal tree species and regions of Canada are equally sensitive to these environmental changes nor are all regions equally affected by anthropogenic disturbance (D'Orangeville et al., 2018; Girardin et al., 2016; Marchand et al., 2018; Ma et al., 2012; Sulla-Menashe et al., 2018). For example, decreases in vegetation productivity are occurring in northwestern boreal forests, whereas southeastern boreal forests show positive trends (Marchand et al., 2018). These complex patterns are likely a product of both regional differences in disturbance regimes and the different sensitivities of the tree genera present in these regions (D'Orangeville et al., 2018; Sulla-Menashe et al., 2018). Arctic vegetation is also responding to unprecedented historical climate change (Box et al., 2019). Increased arctic vegetation productivity such as enhanced shrub growth hypothesized to be a result of warming temperatures, longer growing seasons, deeper thaw depths, increased atmospheric CO_2 concentrations, and increased nutrient availability could lead to greater CO_2 uptake by arctic vegetation (Berner et al., 2020; Jia et al., 2009; Myers-Smith et al., 2020; Tape et al., 2006). This growth may offset some of the anticipated C emissions from the warming and thawing of arctic permafrost soils (Miner et al., 2022; Schuur et al., 2015; Schuur & Mack, 2018). At present, the representation of vegetation within Canada's boreal forests, and tundra ecosystems is limited in regional-scale simulations, restricting our ability to disentangle the impacts of these various

processes and make projections (Friedlingstein et al., 2019; Melton et al., 2020; Meyer et al., 2021; Sulman et al., 2021; Wullschleger et al., 2014).

To date, we are not aware of a comprehensive, process-based assessment of Canada's terrestrial C cycle. Preexisting regional or global C cycling assessments using process-based models, have a relatively coarse spatial resolution (0.5° or more) and have a limited representation of region-specific vegetation types, disturbance, and ground surface-related processes (Chaste et al., 2017; Friedlingstein et al., 2019; Hayes et al., 2012; Huntzinger et al., 2012; Peng et al., 2014). Inventory-based estimates, atmospheric inversion (top-down) models, and data-driven models have been used to estimate C fluxes and stocks in Canada, in some cases at extremely high resolution (1 km or less) but each with their own limitations (Chen et al., 2000, 2003; Ju & Chen, 2008; Kurz et al., 2009; Shiga et al., 2018; Sothe et al., 2022; Xiao et al., 2014). The inventory-based approach cannot disentangle the relative contributions of CO_2 fertilization and climate to vegetation growth, the inversion approach operates at coarse regional resolution, and the data-driven approach is dependent upon the quality of the training data and has difficulty disentangling CO_2 fertilization and climate impacts on vegetation. All three alternative approaches additionally have a limited ability to make future projections. Conversely, regional processes-based models have several advantages that can circumvent some of the drawbacks of the other approaches. They can run at high resolution compared to their global counterparts, include model parameters optimized based upon region-specific data, include regional PFTs that better capture the distribution of vegetation on the landscape, and utilize region-specific data sets (i.e. meteorological or disturbance history drivers) (Koca et al., 2006; Kuntoro et al., 2009; Morales et al., 2007; Santini et al., 2014; Seiler et al., 2014, 2015). Developing a higher resolution process-based model tailored to the pan-Canadian domain is an important step toward disentangling the impact of different processes on Canada's net C balance and projecting how the Canadian C cycle will respond to future climate change.

Representing the distribution and plant traits of Canada's vegetation will improve our capacity to model the Canadian terrestrial C cycle. Plant functional types (PFTs) are commonly used in land surface models (LSMs) to represent broad groups of vegetation with similar characteristics such as their growth form, phenological patterns, or photosynthetic pathways (Bonan et al., 2002; Box, 1996; Smith et al., 1993; Ustin & Gamon, 2010). There are, however, large differences in the coverage and type of PFTs used in LSMs, which in turn impact the simulated fluxes of matter and energy from the land surface (Fritz et al., 2011; Hartley et al., 2017; Ottlé et al., 2013; Wang et al., 2022). Moreover, the PFTs used in LSMs have historically been developed to represent global patterns of vegetation and their associated traits (Bonan et al., 2002; Box, 1996; Melton et al., 2020; Wullschleger et al., 2014). Region-specific PFTs can enhance model realism, more accurately represent the diversity of vegetation on the landscape, and include more informed parameterizations that act to reduce regional biases (Curasi et al., 2022; Epstein et al., 2001; Mekonnen et al., 2021; Meyer et al., 2021; Peng et al., 2014; Rezende et al., 2016; Rogers, 2014). For these region-specific PFTs to improve model performance and robustness they

require sufficient data or expert knowledge to inform their parameterization and specify their distribution. Adding a region-specific PFT increases the number of parameters used in the model. Therefore region-specific PFTs must be carefully specified by balancing realism and parsimony and avoiding issues of equifinality (Anderegg et al., 2022; Prentice et al., 2015). Currently, CLASSIC and indeed we are not aware of any other LSMs that include PFTs tailored to explicitly represent Canada's boreal forests, tundra sedges, and shrubs (Melton et al., 2020; Meyer et al., 2021; Wullschleger et al., 2014).

In this study, we tailor CLASSIC to the pan-Canadian domain by improving its representation of the distribution and traits of Canada's vegetation to enhance CLASSIC's representation of the Canadian C cycle. Given the wide array of vegetation cover products that exist for Canada, we evaluate the performance of CLASSIC when run with prescribed land cover from four vegetation cover products. We also evaluate the impact of including five new PFTs in CLASSIC including shrub, sedge, and region-specific tree PFTs. We compare our offline model simulations to independent remotely sensed and data-driven products to demonstrate the skill of the region-specific model configuration in representing the pan-Canadian domain relative to the standard model setup. Finally, we evaluate the model biases to determine where to implement future improvements.

2. Methods

2.1 The CLASSIC model

CLASSIC is the community open-source successor to the coupled Canadian Land Surface Scheme (CLASS) (Verseghy, 2017, 2000, 2007; Verseghy et al., 1993) and Canadian Terrestrial Ecosystem Model (CTEM) (Arora, 2003; Melton & Arora, 2016). A detailed description and evaluation of CLASSIC v1.0 can be found in Melton et al., (2020) and Seiler et al., (2021). The description below highlights updates since CLASSIC v1.0 that include or improve the representation of certain processes. Within CLASSIC, CLASS simulates the energy and water balances of the land surface and CTEM simulates the biogeochemical processes.

CLASS is the physics sub-model that, when driven by meteorological data, simulates the fluxes of heat, momentum, and water on and within the land surface. CLASS simulates four possible subareas within each grid cell: bare ground, snow-covered ground, canopy-covered ground, and snow-covered canopy, typically on a thirty-minute time step in offline simulations. The model is set up to use 20 ground layers which gradually increase from ten layers of 0.1 m thickness to a 30 m thick layer for a total depth of over 61 m. CLASS simulates water fluxes between the soil layers down to the depth of the underlying impermeable bedrock layers. The water fluxes use an improved first-order Lagrange interpolation to discretize the Richards equation for unsaturated vertical flow (MacKay et al., 2022). CLASS simulates heat transfer within all ground layers including the underlying bedrock. The soil textures and permeable depth used within the model

come from the SoilGrids250m data set (Hengl et al., 2017). CLASS models the canopy as a single layer and in the default configuration uses four plant functional types for the model physics: needleleaf trees, broadleaf trees, grasses, and crops. One of our model runs includes one new region-specific CLASS PFT in addition to those described above: Broadleaf shrubs (see section 2.4 below; Table 1).

CTEM is a dynamic vegetation model which simulates the biogeochemical processes within CLASSIC. CLASS is coupled to CTEM on a daily time step. CLASS provides CTEM with information about the mean daily soil moisture, soil temperature, and net radiation on the land surface. CTEM in turn provides CLASS with information about the overlying vegetation including its height, leaf area index (LAI), biomass, and rooting depth. The vegetation is dynamically simulated by CTEM as a function of environmental conditions through its simulation of photosynthetic fluxes on the physics timestep, and daily simulation of C allocation to three live vegetation components: leaves, stems, and roots. CTEM incorporates non-structural and structural carbohydrate pools within the three live vegetation components (Asaadi et al., 2018). CTEM allocates C first to the non-structural pool, and the model then simulates the flux of C to the structural pool. The non-structural pools buffer the supply of C to improve the seasonality of simulated LAI (Asaadi et al., 2018). CTEM also simulates daily autotrophic respiration (Ra) from the live vegetation components and heterotrophic respiration (Rh) fluxes from the litter and soil C pools. CTEM has a fire module that simulates fires and their associated C fluxes based on climate conditions, population density, and lightning strike frequency (Arora & Boer, 2010; Arora & Melton, 2018). The simulation of the C pools and fluxes within the model utilizes a user-determined number of PFTs. In its default configuration, CTEM utilizes nine biogeochemical PFTs that map onto the physics (CLASS) PFTs (Table 1). One of our model runs utilizes new region-specific CTEM PFTs, in addition to the standard nine, including broadleaf deciduous shrubs, broadleaf evergreen shrubs, continental needleleaf evergreen trees, interior needleleaf evergreen trees, and sedges (see section 2.4 below; Table 1).

2.2 Meteorological forcings and simulation protocol

CLASSIC requires seven meteorological forcing variables for its simulation of matter, energy, and momentum exchanges between the land surface and the atmosphere: incoming shortwave radiation, incoming longwave radiation, air temperature, precipitation rate, air pressure, specific humidity, and wind speed. As described by Meyer et al. (2021), the daily meteorological forcing used in our simulations is from a merged dataset (GSWP3–W5E5–ERA5). The 1901 – 1978 portion of the meteorological forcing comes from the Inter-Sectoral Impact Model Intercomparison Project 0.5° GSWP3–W5E5 bilinearly interpolated to a 0.25° grid (Kim, 2017; Lange, 2019, 2020a, 2020b). The 1979–2018 portion comes from the 0.25° ERA5 time series bias corrected to match the means of the overlapping period of the GSWP3–W5E5 dataset (ECMWF, 2019). We nearest neighbor interpolated the bias-corrected meteorological forcing to

a 0.22° common grid using the Climate Data Operators suite (Schulzweida et al., 2006). We disaggregated the meteorology from daily to half-hourly time steps following the methodology of Melton and Arora (2016) except for incoming longwave radiation which was linearly interpolated. The fire module utilizes time-varying lightning-to-ground strike data from the Optical Transient Detector (OTD) and Lightning Imaging Sensor (LIS) Climatology Data Set (Cecil et al., 2014) and time-varying population density from the Trends in the land carbon cycle 2021 (TRENDY) protocol based on the History database of the Global Environment (Hyde) version 3.2 (Chini et al., 2021; Friedlingstein et al., 2022).

In our simulations, we prescribe the spatial distribution of PFTs using four different land cover products to better elucidate the influence of the new PFTs (see sections 2.3, and 2.4 below). CLASSIC's fire module simulates fires and their associated C fluxes during our model runs. Although CLASSIC can simulate nitrogen (N) cycling and land use change (LUC), we did not use either in these simulations (Arora & Boer, 2010; Asaadi & Arora, 2021).

The model simulations utilize a standard protocol consisting of a spin-up to allow the model to equilibrate C fluxes to conditions corresponding to the year 1850 and a transient run over the period 1850 to 2017. During spin-up, we loop climate data from the earliest 25 years available (1901 - 1925) and hold atmospheric CO_2 concentrations at the pre-industrial level (286.46 ppm). The transient runs use time-varying CO_2 and climate. The early phase of the transient run (1850 - 1900) uses the same 1901 - 1925 climate as the spinup, but with time-varying atmospheric CO_2 concentrations. The later phase of the transient run uses time-varying atmospheric CO_2 concentrations and evolving climate from the 1901–2017 period. The fire module is active during the simulations and during the transient run where it uses the time-varying lightning strike and population density data.

2.3 Land cover products

We use four different land cover products to explore their impact on CLASSIC's ability to represent C cycling-related processes over Canada: Global Land Cover 2000 land cover (GLC 2000), North American Land Change Monitoring System land cover (NALCMS), European Space Agency Climate Change Initiative land cover (ESA CCI), and a hybrid land cover with the default 9 CLASSIC PFTs (Hybrid-9PFT). GLC 2000 is a 1 km resolution global land cover product with 22 classes. It was generated by Bartholomé and Belward (2005) from Satellite Pour l'Observation de la Terre VEGETATION (SPOT-VEG) data collected from November 1999 to December 2000 using an unsupervised image classification method. NALCMS is a 30 m resolution North American regional product with 19 classes (Latifovic et al., 2017). It was generated by the Canada Center for Remote Sensing from Landsat imagery using a random forest algorithm and local optimization method. ESA CCI is a 300 m resolution global product with 22 classes and 15 sub-classes (European Space Agency, 2017). It was generated by the

(European Space Agency, 2017) by applying a combination of machine learning and unsupervised image classification methods to three products: Environmental Satellite (ENVISAT; 2003-2012), SPOT-VEG (1999 - 2013), and Project for On-Board Autonomy Vegetation (PROBA-V; 2013 - 2018). Finally, Hybrid is a Canada-specific product generated by Wang et al. (2022). It combines NALCMS with a land cover classification generated by Hermisilla et al. (2018) using the Virtual Land Cover Engine (VLCE). The VLCE product was generated with a random forest-based classification method using Landsat time-series data and informed by forest change and digital elevation information derived from the Advanced Spaceborne Thermal Emission and Reflection Radiometer (ASTER). The Hybrid product has 17 classes and blends the detailed land cover classification of NALCMS with a more accurate forest cover mapping by VLCE (Wang et al., 2022). Based on field survey data and expert knowledge of global biomes and class descriptions, we use cross-walking tables to convert each dataset's land cover classes into the nine default PFTs in CLASSIC (Table 1) (Wang et al., 2006, 2019, 2022). Information about shrub fractional cover is available in the underlying Hybrid product, however, the default nine PFTs do not include shrubs so we assign a fraction of the shrub cover to the tree PFTs and the remainder to the C3 grass PFT in Hybrid-9PFT.

2.4 Additional PFTs

We implement five additional plant functional types and evaluate how region-specific PFTs improve CLASSIC's performance in Canada and increase the model's realism. Three of the additional PFTs are non-tree PFTs including broadleaf evergreen shrubs, broadleaf deciduous shrubs, and sedges. These PFTs represent shrubs and sedges in Canada's arctic and boreal ecosystems. They were parameterized and extensively evaluated at a high Arctic eddy-covariance tower site by Meyer et al. (2021). We specify the fractional coverage of these three PFTs by creating a cross-walking table for the Hybrid product that includes 12 PFTs (i.e. the default nine plus the three non-tree new PFTs; Table S1) (Wang et al., 2006, 2019, 2022).

The other two additional PFTs are needleleaf trees: continental needleleaf evergreen trees and interior needleleaf evergreen trees. The interior needleleaf evergreen tree PFT parameterization comes from Peng et al. (2014) and assumes 50% lower rates of leaf loss from cold and drought in the CTEM phenology model compared to the standard needleleaf evergreen tree PFT (Table 1). This PFT roughly corresponds to the pines (*Pinus* spp.), spruces (*Picea* spp.), subalpine fir (*Abies lasiocarpa*), interior Douglas fir (*Pseudotsuga menziesii* var. *glauca*), western hemlock (*Tsuga heterophylla*), and western red cedar (*Thuja plicata*) that occupy the interior of British Columbia. We specify the fractional cover for this PFT by splitting the interior needleleaf evergreen PFT from the needleleaf evergreen tree cover in the 12 PFT version of Hybrid using land cover classifications encompassing these species or subspecies in British Columbia's biogeoclimatic ecosystem classification map (MacKenzie & Meidinger, 2018; Salkfield et al., 2016). The continental needleleaf evergreen tree PFT parameterization is based on Qu et al.,

(2021) and has a lower maximum carboxylation rate of Rubisco (V_{max}; Table 1) than the default needleleaf evergreen tree PFT. This PFT primarily corresponds to black spruce (*Picea mariana*), which occupies the continental interior of Canada. We calculate the fraction of the total needleleaf evergreen tree cover that is white or black spruce using gridded species composition data from Canada's National Forest Inventory for areas within Canada, and from the Scenarios Network for Alaska and Arctic Planning for areas within Alaska (Beaudoin et al., 2018; *Land Cover v0.2*, 2021). To estimate the fractional cover of the continental needleleaf evergreen PFT, we apply this fractional value to the needleleaf evergreen tree cover in the 12 PFT version of Hybrid. The resulting land cover product and associated model runs are hereafter referred to as the Hybrid land cover with 14 PFTs (Hybrid-14PFT).

2.5 Reference data sets

We evaluate the CLASSIC outputs against in situ and gridded observation-based data (hereafter termed reference data) available within the pan-Canadian domain. The 33 reference data sets contain information about 12 variables relevant to the energy, C, and water cycle including above-ground biomass (AGB), the fraction of area burnt (BURNT), gross primary productivity (GPP), latent heat flux (HFLS), leaf area index (LAI), net surface longwave radiation (RLS), net surface radiation (RNS), net surface shortwave radiation (RSS), sensible heat flux (HFSS), shortwave albedo (ALBS), snow water equivalent (SNW), and soil carbon (CSOIL). These data sets include either monthly mean values or are simply a snapshot in time (Table 2) and are versions of those detailed in Seiler et al., (2021, 2022) which we interpolated to the 0.22° model grid. Our analysis focuses on AGB, CSOIL, GPP, and LAI as these variables are particularly relevant to the C cycle and multiple gridded reference data sets are available for each which allows us to consider observational uncertainty.

The GPP reference data sets are from the Moderate Resolution Imaging Spectroradiometer (MODIS) (Zhang et al., 2017), the FluxCom initiative (FluxCom) (Jung et al., 2019), the Global Orbiting Carbon Observatory-2 Solar-induced Chlorophyll Fluorescence (GOSIF) (Li & Xiao, 2019), and the Global Land Surface Satellite Product Suite (GLASS) (Liang et al., 2021). MODIS GPP was calculated from a range of MODIS and reanalysis products using a light-use efficiency model which considers the efficiency with which vegetation uses light absorbed by chlorophyll to fix carbon via photosynthesis. GOSIF GPP was calculated based on a statistical model which relates GPP measurements from eddy covariance towers to solar-induced chlorophyll fluorescence (SIF) from the global Orbiting Carbon Observatory-2 (OCO-2). FluxCom GPP was upscaled from eddy covariance towers using an ensemble of six machine learning models and an array of MODIS-derived remotely sensed products and meteorological data from the Climate Research Unit National Centers for Environmental Prediction version 8. We pre-process FluxCom GPP by calculating the median of the six ensemble members. GLASS GPP was calculated from a range of remotely sensed products detailing direct and diffuse

radiation fluxes, vapor pressure deficit, and atmospheric CO_2 concentrations using an eddy covariance-derived light use efficiency model. All of these GPP data sets directly integrate or were originally validated against eddy covariance tower data which exhibits some spatial bias against far north regions in its sampling distribution (Jung et al., 2020; Keenan & Williams, 2018).

The LAI reference data sets are from MODIS (Myneni et al., 2002), the Advanced Very High-Resolution Radiometer (AVHRR) (Claverie et al., 2016), and the European Space Agency's Copernicus Global Land Service (Copernicus) (Verger et al., 2015, 2016). The LAI reference data sets were all derived from surface reflectance based on satellite imagery. MODIS LAI was calculated by inverting a three-dimensional canopy radiative transfer model. Claverie et al., (2016) derived AVHRR LAI from AVHRR surface reflectance using an artificial neural network trained using LAI from MODIS (MCD15A2) and calibrated using in situ data from Baret et al., (2006). Finally, Copernicus LAI was generated from SPOT-VEG satellite imagery using an artificial neural network. The Copernicus LAI product was filtered to remove artifacts due to snow cover or poor illumination. At high latitudes, an additional correction was applied where the pixels were fixed at their minimum values when the sun's zenith angle was >70°. Gap-filling was also applied, but our analysis only uses non-gap-filled records.

The AGB reference data sets come from the Global Carbon Observation and Analysis System (GEOCARBON) (Avitabile et al., 2016; Santoro et al., 2015), Huang et al., (2021) (Huang2021), Canada's National Forest Inventory (NFI) (Gillis et al., 2005), Zhang et al., (2020) (Zhang), and in-situ observations from Schepaschenko et al., (2019) and Xue et al., (2017) (FOSXue). These AGB reference data sets are diverse both in terms of the methodologies applied and the underlying field data or remote sensing covariates used. GEOCARBON AGB was created by harmonizing two pre-existing AGB data sets from Santoro et al., (2015) for boreal regions and Avitabile et al., (2016) for tropical regions. Therefore in our region of interest, it is primarily informed by the Envisat Advanced Synthetic Aperture Radar (SAR) derived estimates of Santoro et al., (2015). Huang2021 AGB was developed from Santoro et al., (2018) which, in turn, was derived from Advanced Land Observing Satellite and Envisat SAR. The SAR retrievals were used to estimate the volume of wood on the landscape. Then AGB was calculated based on wood density and a biomass expansion factor derived by upscaling in-situ data. When validated against in-situ data, Huang2021 AGB performed better in boreal regions than in tropical, subtropical, and temperate regions (Santoro et al., 2021). Zhang AGB used data fusion to integrate 10 pre-existing aboveground biomass maps that were then extensively evaluated against in-situ observations and LIDAR observations. The pre-existing AGB products fused in Zhang exhibit large differences in AGB in boreal regions and positive biases globally. FosXue and NFI AGB are both in-situ point-based reference data sets that were derived by upscaling field measurements using allometric equations. The NFI has excellent spatial coverage of forested areas within Canada and consists of approximately 20,000 plots located on a 20 x 20 km grid.

The FOSXue data combined in-situ observations from Xue et al., (2017) and Schepaschenko et al., (2019). It has fairly limited spatial coverage within Canada encompassing <50 sites concentrated in southern forests.

The CSOIL reference data sets come from the Harmonized World Soil Database (HWSD) (Todd-Brown et al., 2013), and the SoilGrids system at 250m resolution (SG250m) (Hengl et al., 2017). HWSD CSOIL was created by combining soil survey data with the FAO Soil Map of the World to calculate the soil C content of the top 100cm of soil. SG250m CSOIL was created by upscaling 150,000 soil survey data records using an ensemble of machine learning models and 150 remotely sensed covariates. We process SG250m to only include the first 100cm of soil and make it comparable to HWSD. These two data sets are known to differ in the extent to which they represent peatlands, river floodplains, and permafrost soils leading to lower CSOIL in HWSD when compared to SG250m (Seiler et al., 2022; Tifafi et al., 2018).

The BURNT reference data sets come from the Global Fire Emissions Database (GFED4S) (Giglio et al., 2013), and the European Space Agency Climate Change Initiative land cover (ESACCI) (Chuvieco et al., 2018). The SNW reference data sets come from a blended product developed at Environment and Climate Change Canada (ECCC) which combines four other gridded SNW products (Brown et al., 2003; Brun et al., 2013; Gelaro et al., 2017; Takala et al., 2011), and in-situ SNW measurements compiled by Mortimer et al., (2020) (Mortimer). The surface energy balance-related reference datasets come from the Clouds and the Earth's Radiant Energy System (CERES) (Kato et al., 2013), the Global Energy and Water Cycle Experiment-Surface Radiation Budget (GEWEXSRB) (Zhang et al., 2011), the Conserving Land–Atmosphere Synthesis Suite (CLASSr) (Hobeichi et al., 2020), FluxCom and MODIS (Strahler et al., 1999).

2.6 The Automated Model Benchmarking R package

The Automated Model Benchmarking R package (AMBER*)* assesses model performance against the reference data sets and calculates skill scores (Seiler et al., 2021). The package calculates a total of six scores: the bias score (S_{bias}), the root-mean-square-error score (S_{rmse}), the phase score (S_{phase}), the interannual variability score (S_{iav}), the spatial distribution score (S_{dist}), and the overall score ($S_{overall}$). S_{bias} assesses the difference between the reference and modeled mean values. S_{rmse} evaluates the residuals of the reference and modeled time series. S_{phase} assesses how well the model reproduces the seasonality in the reference time series. S_{iav} assesses how well the model reproduces the interannual variability in the reference time series. S_{dist} evaluates how well the model captures the pattern of a variable across space compared to the reference data. Finally, $S_{overall}$ is a weighted average of the other five scores where S_{rmse} is weighted by a factor of two commensurate with its perceived importance in assessing model performance. The scores are dimensionless and on a scale from 0 to 1. The scores express the level of agreement between the

model and reference data with a higher value implying better performance. Lower values are, however, not necessarily a product of poor model performance as the scores are also affected by uncertainties in the forcing and reference data. Further details regarding the AMBER R package as well as the skill score equations are presented in Seiler et al. (2021) and Seiler (2019).

We also calculate benchmark scores for the reference data sets compared to one another. These scores quantify the level of agreement between the reference data sets. They are indicative of the $S_{overall}$ that is achievable given the uncertainty between the reference data sets. The benchmark scores for a single variable (i.e. GPP) can vary among the reference data sets due to the calculations involved in normalizing each statistical metric (Seiler et al., 2022). If the model skill scores reach the benchmark scores then the level of disagreement between the model and the reference data set is of similar magnitude to the uncertainty between the individual reference data sets. The model scores can exceed the benchmark scores when the model falls within the uncertainty range of the reference data.

3. Results

3.1 The spatial distribution of land cover

The four vegetation cover products differ in terms of the fractional cover of the 9 CTEM PFTs and their dominance. In all four land cover products, needleleaf deciduous trees, broadleaf drought/dry deciduous trees, C4 crops, and C4 grasses PFTs are for the most part found at lower latitudes and are not present or have a negligible fractional cover in the pan-Canadian domain (Figure S1). The broadleaf evergreen tree PFT is only present in GLC 2000 and ESA CCI, with limited fractional cover (Figure S1a,c).

Needleleaf evergreen trees dominate western and mid-latitude Canada, whereas broadleaf cold deciduous trees dominate southern Ontario and Quebec (Figure 1). The fractional cover of needleleaf evergreen and broadleaf cold deciduous trees is generally higher in GLC 2000 when compared to the other three land covers. C3 crops dominate southeastern and south-central Canada, however, the fractional cover of C3 crops is lower in GLC 2000 (Figure 1a) than in the other three data sets (Figure 1b-d). C3 grass is dominant in parts of south-central Canada and the Arctic; however, its fractional cover differs widely between the four data sets. In GLC 2000, C3 grass cover in south-central Canada is higher and more widespread, likely due to its lower C3 crop cover when compared to the other three data sets (Figure 1a). GLC 2000 also uses a mix of C3 grass and broadleaf cold deciduous trees at high latitudes (Figure 1a). ESA CCI has consistent C3 grass cover at higher latitudes (Figure 1c) whereas NALCMS and Hybrid-9PFT feature a peak ~70° north and a gradual decline in C3 grass cover at higher latitudes (Figure 1b,d).

3.2 Comparisons of model simulations with different PFT cover

The AMBER scores of the CLASSIC model runs using the four different prescribed PFT covers vary when compared to an array of reference data sets (Figure 2). The model run using Hybrid-9PFT has the best overall performance for C cycling-related reference data sets. Hybrid-9PFT has the highest overall score for three out of the four GPP reference data sets with an average improvement of 0.013 when compared to the land cover with the lowest score (Figure 2 b,c). Similar improvements are seen for LAI (3/3 data sets), AGB (2/5 data sets), and CSOIL (2/2 data sets). These improvements are primarily a result of improvements in the spatial distribution (S_{dist}) of these C cycling variables and in the bias (S_{bias}; Figure 2b). The overall score differences are generally large ranging from 0.02 to 0.08. The NALCMS and ESA CCI model runs rank second or third against C cycling-related reference data sets with approximately equal frequency (Figure S2). The score differences between the first and second-ranked model runs are often small (i.e. <0.01) but are eclipsed by large differences between the first and third-ranked model runs (i.e. >0.01).

ESA CCI consistently improves the model's performance in terms of surface energy balance-related comparisons and has the highest overall score for RNS (3/4 data sets) and ALBS (3/3 data sets; Figure 2 b,c). These improvements are primarily due to changes in the spatial distribution of RNS and ALBS (Figure 2c). The differences in the overall scores are lower ranging from <0.01 to 0.03. The Hybrid-9PFT and NALCMS often rank second and third against these surface energy balance-related data sets and exhibit similar performance when compared to the top-ranked model run (i.e. score differences <0.01; Figure S2). Looking across all of the comparisons, GLC 2000 is the lowest-scoring land cover (22/33 comparisons; Figure 2d).

Average AGB ranges from 1.9 to 5.7 kg C m^{-2} in the various gridded reference data sets masked to the same spatial extent. In the point data average, AGB is 6.0 kg C m^{-2} for FosXue, and 4.6 kg C m^{-2} for NFI. The spatial extent of the FosXue data, which is concentrated in southern Canada, is markedly different from that of the NFI data, which covers most forested areas in Canada (Figure S3). The NFI point data has the widest range of any AGB reference data set (0 - 36.7 kg C m^{-2}; Figure S3). The model runs fell into a smaller range towards the higher end of that found within the reference data (4.3 - 5.0 kg C m^{-2}). In both the model runs and the reference data, AGB generally declines with increasing latitude (Figure 3a). For the model simulations, the slope of this decline is steepest for GLC 2000. Average CSOIL ranges from 15 - 50 kg C m^{-2} in the various reference datasets while the model runs fall into a small range (13 - 17 kg C m^{-2}) at the lower end of the reference data. The model-simulated CSOIL is generally similar to the HWSD reference data set from 45° - 65° north but has lower values at higher latitudes (Figure 3b). The CSOIL reference datasets differ dramatically amongst themselves at mid to high latitudes with HWSD consistently lowest. The average GPP in the various reference data sets ranges from 1.3 - 1.7 g C m^{-2} day^{-1} while the model simulates a smaller range from 1.4 - 1.5 g C

506 m^{-2} day^{-1}. GPP declines with increasing latitude in both the model runs and the reference data
507 sets (Figure 3c). The model generally estimates higher GPP than the reference data sets at <60°
508 north and is within the range of reference data sets at higher latitudes. GLC 2000 has the steepest
509 decline in GPP with increasing latitude. The average LAI in the various reference data sets
510 ranges from 0.9 - 1.3 m^2 m^{-2} and the model runs fall into a smaller range from 1.4 - 1.5 m^2 m^{-2}.
511 All the model runs have higher LAI than the reference data from 45° - 60° north. The Copernicus
512 reference data is substantially closer to the modeled values than MODIS or AVHRR (Figure 3d).
513
514 *3.3 Additional plant functional types*
515
516 The Hybrid-14PFT vegetation cover product has more heterogeneous vegetation cover patterns
517 than the baseline Hybrid-9PFT. In Hybrid-14PFT, needleleaf deciduous, broadleaf drought/dry
518 deciduous, and broadleaf evergreen trees are again not present in Canada whereas some limited
519 C4 crop cover is present in central Canada and southern Ontario (Figure S4). Needleleaf
520 evergreen trees in Hybrid-9PFT are largely replaced by continental needleleaf evergreen trees in
521 the central mid-latitudes of Canada and interior needleleaf evergreen trees in western Canada in
522 Hybrid-14PFT (Figure 4a,b). C3 grass PFT cover is largely replaced by broadleaf deciduous, and
523 to a lesser extent, broadleaf evergreen shrub cover throughout Canada. In Hybrid-14PFT, the
524 Arctic is now dominated by a mix of sedge, broadleaf deciduous shrub, and broadleaf evergreen
525 shrub cover which replaces the homogenous C3 grass cover in Hybrid-9PFT (Figure 4b). In
526 Hybrid-14PFT, broadleaf deciduous shrubs dominate the low arctic, but their fractional cover
527 declines and is largely supplanted by sedges at high latitudes.
528
529 *3.4 Model performance with additional plant functional types*
530
531 The addition of five CTEM PFTs to the model improves its performance against reference data
532 for several C cycling-related variables (Figure 5). The overall scores for three of the five AGB
533 reference data sets improve between 0.04 and 0.14. This is primarily a result of large
534 improvements (i.e. up to 0.14) in the spatial distribution and bias of modeled AGB (Figure 5 b,c)
535 This came at the cost of a performance loss against the Zhang and FOSXue reference data. The
536 overall scores for three of the four GPP reference data sets also improve by between 0.04 and
537 0.06 due to improvements in the spatial distribution, interannual variability, and bias of modeled
538 GPP. GLASS is the only GPP reference data product to show an overall score decrease with
539 Hybrid-14 over Hybrid-9. Changes in the spatial distribution of CSOIL lead to a decrease in
540 performance against both CSOIL reference data sets. The overall scores now meet or exceed the
541 benchmark scores for most GPP (4/4) and AGB (4/5) reference data sets, but fewer CSOIL (1/2)
542 and LAI (0/3) reference data sets (Figure 6). The C cycling-related overall scores consistently
543 exceed the original GLC 2000 model run, except for CSOIL (Figure 6, S5, S6).
544

There are smaller (i.e. <0.1) changes in the overall scores of surface energy balance-related variables except for latent heat flux (HFLS) where changes in its modeled distribution and inter-annual variability lead to overall score declines between 0.03 and 0.04 (Figure 5b,c). The HFLS overall scores nonetheless still exceed the benchmark scores for both reference data sets (Figure 6).

The AGB for CLASSIC simulations with 14 PFTs is lower on average (3.1 kg C m^{-2}) than that with 9 PFTs (4.5 kg C m^{-2}). There is a similar decline in AGB with increasing latitude in both, but with 14 PFTs, the model is now closer to the middle estimate provided by the reference data (Figure 7a). With 14 PFTs, CLASSIC simulated CSOIL (11 kg C m^{-2}) is also lower on average than simulations with 9 PFTs (16 kg C m^{-2}). Both model runs generally cluster around the HWSD CSOIL reference data (Figure 7b). With the 14 PFTs, CLASSIC simulated GPP is lower on average (1.1 g C m^{-2} day^{-1}) than estimated with the 9 PFTs (1.4 g C m^{-2} day^{-1}). The additional PFTs move GPP to within the range of the reference data at <60° north, where the model run with 9 PFTs generally is above the range of the reference data (Figure 7c). The simulated LAI with the 14 PFTs CLASSIC run is lower on average (1.1 m^2 m^{-2}) than with 9 PFTs (1.4 m^2 m^{-2}) and is biased low compared to the Copernicus reference data from 45° - 60° north (Figure 7d).

Use of the 14 PFT land cover and associated parameterizations in CLASSIC significantly reduces regional biases in simulated AGB, GPP, and LAI across Canada (Figure 8). With the 14 PFTs model setup, AGB, CSOIL, and GPP are within the 95% confidence interval of the gridded reference data across the majority of Canada (Figure 8). Exceptions include interior British Columbia where the model under-predicts AGB (Figure 8a) and southeastern and south-central Canada where GPP exhibits significant negative biases (Figure 8c). CSOIL did not exhibit distinct regional biases between the two model runs and large disagreements between the two reference data sets likely confound the CSOIL significance tests (Figure 8b). The largest absolute bias in CSOIL occurs in the Hudson Bay Lowlands region. Modeled LAI and BURNT exhibit strong, often significant biases across much of Canada in both model runs. With the CLASSIC 14 PFTs simulation, strong positive LAI biases remain in boreal and western Canada (Figure 8d). BURNT exhibits consistent strong negative biases in the mid-latitude boreal region of Canada and strong positive biases in the plains region (Figure 8e). BURNT falls outside the 95% confidence interval of the reference data across the majority of Canada in line with its low scores (Figure 5, 6, S6).

4. Discussion

We evaluate CLASSIC's performance across the pan-Canadian domain and demonstrate its skill at simulating C cycling at regional scales. Comparing CLASSIC runs using different prescribed PFT covers demonstrates the model's sensitivity to prescribed vegetation cover (Figure 1-3). The addition of five region-specific PFTs further improves CLASSIC's skill at simulating regional C

cycling compared to the 9 PFT model runs and demonstrates that a well-informed regional parameterization can reduce biases (Figure 4-8). For Hybrid-14PFT, the overall scores ($S_{overall}$) for the majority of C-cycling (9/14) and many surface energy balance (7/15) processes meet or exceed the benchmark scores, further highlighting the skill of our regional parameterization (Figure 6, S5, S6). Some processes (i.e. LAI, CSOIL, BURNT) continue to exhibit biases similar to those observed in CLASSIC and other LSMs at global scale (Figure 8b,d,e) (Seiler et al., 2022).

4.1 Vegetation cover impacts the modeled C cycle

Differences in the distribution and fractional cover of PFTs can impact an LSM's simulated fluxes of matter and energy (Fritz et al., 2011; Gou et al., 2019; Hartley et al., 2017; Jung et al., 2007; Ottlé et al., 2013; Quaife et al., 2008; Wang et al., 2022). Our results clearly demonstrate CLASSIC is sensitive to differences in prescribed PFT cover which produce wide-ranging impacts across the model outputs. GLC 2000 exhibits consistently higher tree PFT cover and lower crop and grass cover than other land cover products (Figure 1). The higher tree PFT cover biases the simulated fluxes of matter and energy in the model resulting in the GLC 2000 run consistently scoring the lowest (Figure 2). In the GLC 2000 run AGB, GPP, and LAI fall above the range of the reference data sets at mid-latitudes where tree cover is highest, and below the range of the reference data at higher latitudes where C3 grasses are prescribed to dominate (Figure 1-3). CLASSIC is particularly sensitive to mid-latitude differences in prescribed tree cover owing to its parameterization and the growth forms prominent role on the landscape (Huntzinger et al., 2012; Melton et al., 2020; Melton & Arora, 2016). The Hybrid-9PFT run falls near or within the range of the AGB, GPP, and LAI reference data owing to its lower tree cover and gradual decline in C3 grass cover with increasing latitude (Figures 1-3). As a result, the Hybrid-9PFT run consistently scores higher in C cycling-related comparisons. These results demonstrate that the use of realistic land cover products in LSMs can help reduce regional or global C cycling biases.

Differences in the distribution and cover of PFTs are known to be a significant source of uncertainty between LSMs (Hartley et al., 2017; Teckentrup et al., 2021). GLC 2000, which generally is the lowest-scoring run in this study, has been employed in previous versions of CLASS-CTEM (Arora et al., 2009; Wang et al., 2006). It is the oldest and has the lowest spatial resolution of the five land cover products considered here (Bartholomé & Belward, 2005; European Space Agency, 2017; Latifovic et al., 2017; Wang et al., 2022). It also does not include changes in land cover due to disturbance or agricultural land use change, which have occurred since 2000 and are included in the other products. Hybrid-9PFT, on the other hand, is Canada-specific and integrates more recently produced higher-resolution products. Therefore, advances in remote sensing which yield higher resolution, region-specific information, and more accurately characterize the vegetation on the landscape can represent a potential boon for

improving the accuracy of LSM simulations on regional to global scales (Fritz et al., 2011; Lu & Weng, 2007; Macander et al., 2022; Ottlé et al., 2013; Ustin & Gamon, 2010). Methods that blend vegetation cover products with varying extents, classes, or data types could allow global LSMs with regional biases to benefit from these advances (Hartley et al., 2017; Wang et al., 2022, 2017; Zhang & Liang, 2020). Finally, model evaluation methods similar to those employed here i.e., Seiler et al. 2021, Seiler 2019, and Collier et al. 2018, present a powerful tool for determining the impact of different vegetation cover products on LSMs.

4.2 Region-specific PFTs improve the representation of C cycle processes

We also demonstrate that PFTs designed for use in global models can exhibit biases when used in regional scale simulations while region-specific PFTs can reduce these biases by better representing the traits of vegetation on the landscape (Epstein et al., 2001; Harper et al., 2018; Peng et al., 2014; Rezende et al., 2016; Rogers, 2014; Wullschleger et al., 2014). The five additional PFTs in this study address significant sources of bias in AGB and GPP. This is possible because sufficient information is available to inform their incorporation into the model (i.e. Meyer et al., 2021; Peng et al., 2014; Qu et al., 2021; Land Cover v0.2, 2021; Beaudoin et al., 2018). These PFTs have the additional benefit of improving the LAI biases while not exacerbating the existing CSOIL biases when compared to reference data (Figure 5).

In our baseline model runs there is substantial positive bias in AGP, GPP, and LAI across the forested region of central Canada (Figures 6 & 7). This aligns with results by Qu et al., (2021) showing that the default needleleaf evergreen tree PFT in CLASSIC has a high V_{max} which leads to an overestimated GPP when compared to eddy covariance observations in Canadian boreal forest stands (predominantly spruce trees). Incorporating the continental needleleaf evergreen tree PFT reduces these biases (Figures 4, 7, & 8). Similar positive GPP biases in boreal Canada and Eurasia were observed in TRENDY LSMs (Seiler et al., 2022). V_{max} for needleleaf evergreen tree PFTs also varies widely in LSMs (Rogers, 2014). The interior needleleaf evergreen tree PFT more accurately represents the leaf traits of needleleaf evergreen trees within interior British Columbia (BC) and reduces the negative AGB biases in interior BC (Peng et al., 2014; Reich et al., 1995) (Figure 8).

The shrub and sedge PFTs improve model realism in high-latitude regions. These PFTs have been shown to improve the representation of soil temperatures, soil moisture, CO_2, and energy fluxes in tundra ecosystems in site-level simulations (Meyer et al., 2021). The shrub and sedge PFTs more realistically represent the heterogeneous vegetation cover in tundra, which is often modeled using a single C3 grass PFT (Curasi et al., 2022; Meyer et al., 2021; Myers-Smith et al., 2011; Wullschleger et al., 2014). These ecosystems are particularly significant given shrub expansion and complex greening patterns and browning observed across the Arctic (Berner et al., 2020; Jia et al., 2003, 2009; Mekonnen et al., 2021; Tape et al., 2006). Further model evaluation

and meta-analysis will determine if global LSMs will see a similar benefit from these region-specific PFTs.

4.3 Will further regional parameterization improve performance?

While there is significant diversity in tree genera across Canada, data quantifying how this diversity translates into differences in traits and plant function is limited (Beaudoin et al., 2018; Fisher et al., 2018; Iversen et al., 2017; Iversen & McCormack, 2021; Kattge et al., 2020). Additional region-specific PFTs need to be well-informed, ideally by field data, to balance realism and parsimony (Anderegg et al., 2022; Prentice et al., 2015). The addition of five PFTs brings the model runs within the range of available observation-based estimates provided by the AGB, LAI, and GPP reference data (Figures 6 & 7). As a result, further improvements in model performance against one data set are likely to degrade performance against another.

The GPP reference data sets have high benchmark scores but are relatively clustered, possibly due to the similar underlying data sets used to create and validate them (Jung et al., 2019; Liang et al., 2021; Li & Xiao, 2019; Zhang et al., 2017). Hybrid-14PFT exceeds the GPP benchmark scores (Figure 6). The improvements in simulated GPP, especially for latitudes <60° north for three-quarters of the data sets, come at the expense of performance versus GLASS which has generally higher GPP (Figure 5,7c). The AGB data sets have lower benchmark scores and vary more in their estimates possibly due to the diversity of methodologies and underlying data used to create them (Avitabile et al., 2016; Gillis et al., 2005; Huang et al., 2021; Santoro et al., 2015; Schepaschenko et al., 2019; Xue et al., 2017; Zhang & Liang, 2020). Hybrid-14PFT exceeds the AGB benchmark scores in the majority of cases (Figure 6). The improvements in simulated AGB against 3/5 of the reference data sets, likely come at the expense of performance versus the Zhang and spatially limited FOSXue which have higher average AGB (Figure 5,7c).

For LAI, Hybrid-14PFT improves slightly against MODIS and AVHRR at the expense of performance against Copernicus (Figure 5, 7). Hybrid-14PFT approaches but does not yet meet, the benchmark scores for these data sets (Figure 6). There is disagreement between MODIS/AVHRR, which are derived using similar methods, and Copernicus LAI, which employs additional filtering and correction at high latitudes (Claverie et al., 2016; Myneni et al., 2002; Verger et al., 2015, 2016). The positive LAI biases here are similar to those observed by Seiler et al., 2022, but are difficult to interpret given the disagreement between the individual LAI reference data sets. For CSOIL there is disagreement between the reference data due to differences in the extent to which peatlands, river floodplains, and permafrost soils are represented (Seiler et al., 2022; Tifafi et al., 2018) (Figures 6-8). These processes are likewise not represented within the CLASSIC framework used in our study. As a result, Hybrid-14PFT falls close to the values for CSOIL HWSD and exceeds the benchmark score for that data set. Ultimately, efforts to make field data for model parameterization more widely available and to

create more accurate reference data sets are key for further regional parameterization (Kattge et al., 2020; Kyker-Snowman et al., 2021; Seiler et al., 2021, 2022)

Our results highlight areas in which further work could improve model realism and performance in the Canadian domain. First, disturbance processes (i.e. fire, harvest, and insect damage) have significant impacts on the net C balance of Canada's forests (Chaste et al., 2017; Giglio et al., 2013; Giles-Hansen & Wei, 2022; Ju & Chen, 2008; Kurz et al., 2008, 2009; Landry et al., 2016; Weber & Flannigan, 1997; White et al., 2017). Harvest affected 3% of Canada's land mass from 1985 - 2010, and fire affected 7% of Canada's land mass from 1985 - 2010 (White et al., 2017). Insect damage which often does not completely kill and replace stands affected 25% of Canada's land mass from 1990 - 2010 (CCFM: National Forestry Database, 2022). All three of these processes are underrepresented and biased in CLASSIC simulations for Canada (Figure 6, 8). The absence of these disturbance processes likely contributes to the remaining positive AGB, GPP, and LAI biases. Second, despite the large uncertainty in the CSOIL reference data, the largest absolute CSOIL biases are in peatlands (i.e. the Hudson Bay Lowlands) and tundra (Figure 8). These CSOIL biases mirror those observed in other TRENDY models and can likely be improved by explicitly representing peatland, river floodplains, permafrost C, and yedoma (Melton et al., 2019; Seiler et al., 2022; Wu et al., 2016). Future efforts to incorporate disturbance and high latitude soil C processes within CLASSIC in Canada will improve its representation of these globally important soil C pools and Canada's terrestrial C cycle more broadly.

5. Conclusion

Canadian ecosystems are critical components of the global carbon cycle which are responding to unprecedented climate change. We developed the first parameterization of a process-based LSM tailored to Canada. We demonstrate that region-specific vegetation cover products and region-specific plant functional types improve CLASSICs' performance against independent reference data. Our model evaluations show that future work focused on incorporating a parameterization for boreal disturbance processes (i.e. fire and harvest) and explicitly representing peatlands and permafrost soils are important next steps in tailoring CLASSIC for optimal performance over Canada with potential improvements for other boreal regions. We argue that developing further region-specific land cover products, well-informed PFT parameterizations, and more detailed reference data sets will facilitate improvements to the representation of the terrestrial C cycle in regional and global LSMs. Ultimately this is an important step toward a comprehensive process-based assessment of Canada's terrestrial C cycle and understanding the response of Canada's net C balance to climate change

.

6. Acknowledgements:

We would like to thank Mike Brady (ECCC) for his assistance. We acknowledge the support of the Natural Sciences and Engineering Research Council of Canada (NSERC), ALLRP 556430-2020. We also thank the two anonymous reviewers for their constructive comments.

7. Open research statement:

All software used here inclusing the CLASSIC and AMBER code and the resulting model outputs presented here in are archived on Zenodo at https://doi.org/10.5281/zenodo.7199340.

8. Author contributions:

S.R.C., J.R.M., and E.R.H. conceived of the analysis. S.R.C. conducted the modeling analysis. L.W. created the land cover products and cross-walking tables. E.C. set up the model initialization files and meteorological drivers. C.S. set up the Canada domain amber benchmarking suite, A.J.C. bias-corrected the meteorological drivers. B.Q. developed the continental needleleaf evergreen tree parameterization. J.R.M. and E.R.H. obtained funding for the work. All authors contributed to writing and editing the manuscript.

9. Figures

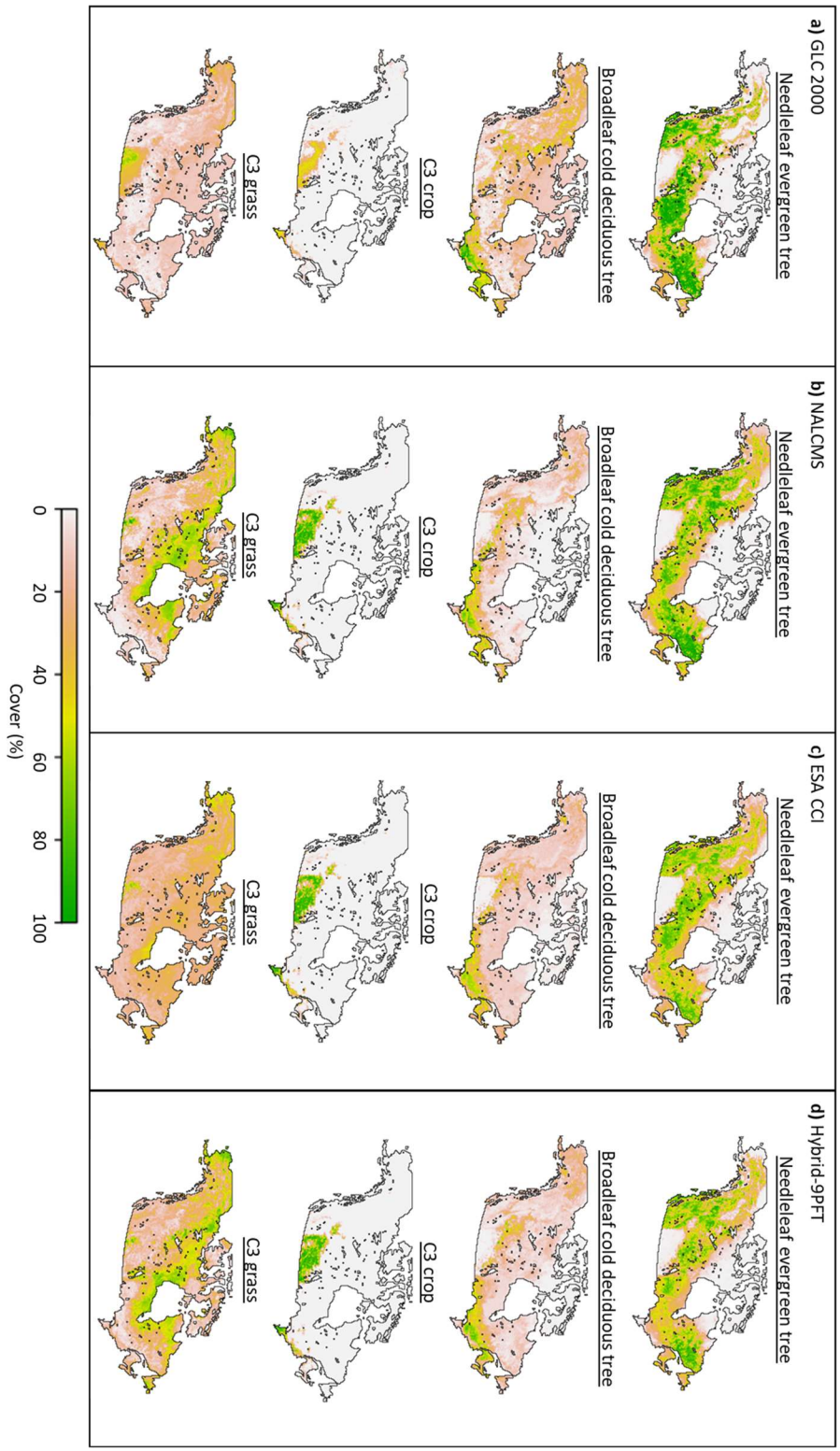

Figure 1: Maps of dominant plant function type (PFT) cover across Canada for **a)** GLC 2000, **b)** NALCMS, **c)** ESA CCI and **d)** Hybrid-9PFT vegetation cover products.

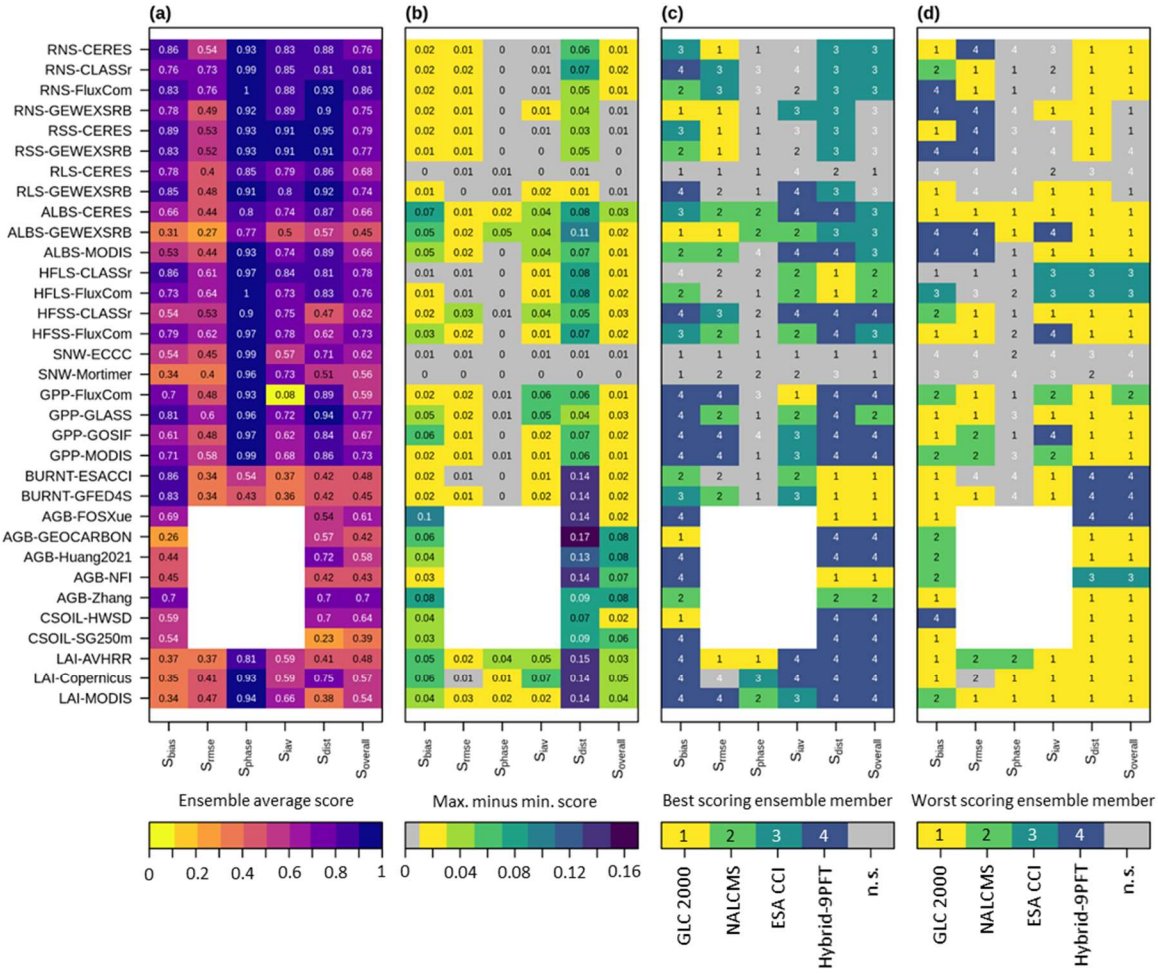

Figure 2: a) Mean ensemble score, **b)** maximum score difference among ensemble members, and ensemble member with the **c)** highest and **d)** lowest score for historical model runs using the GLC 2000 (1), NALCMS (2), ESA CCI (3), and Hybrid-9PFT (4) vegetation cover. Comparisons are greyed out in panels b-d when the difference between the maximum and minimum scores is less than 0.01. S_{rmse}, S_{phase}, and S_{iav} are omitted for reference data sets that are a snapshot in time

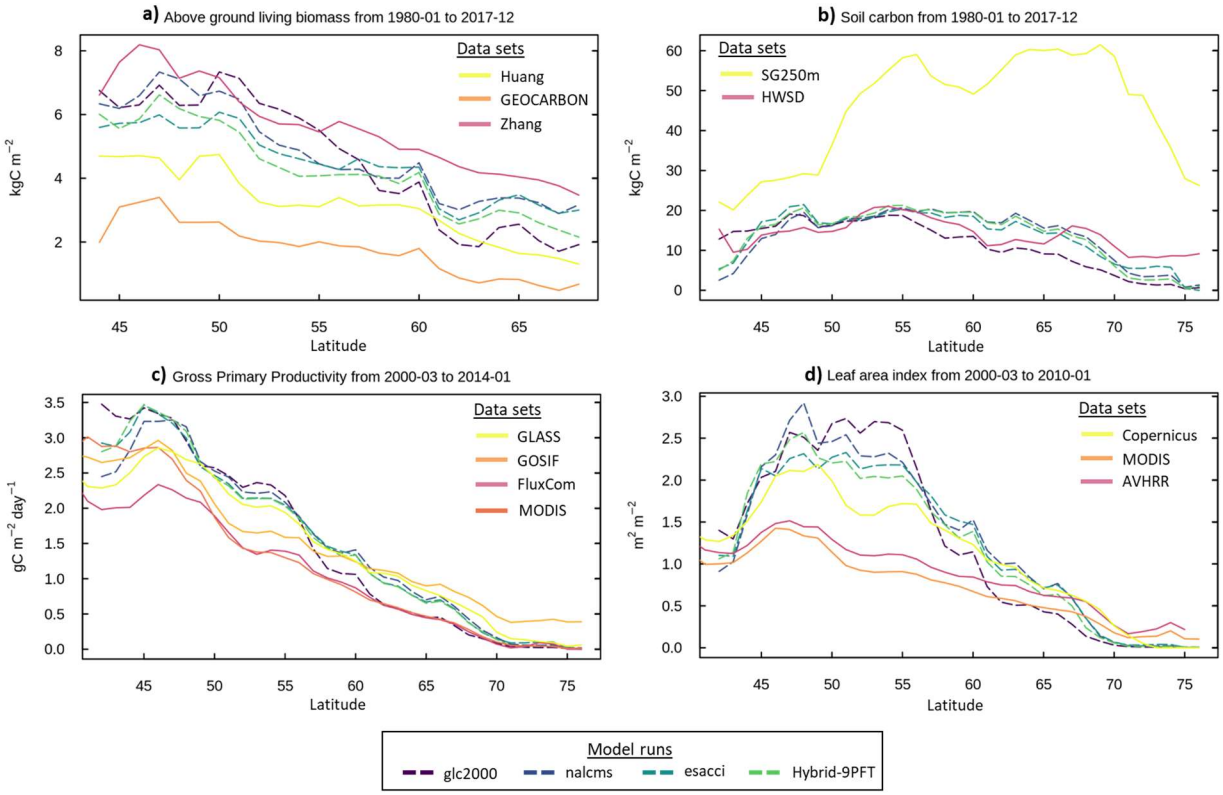

774

775 **Figure 3:** Plots of the zonal average of **a)** Above ground living biomass (AGB) **b)** Soil carbon
776 (CSOIL) **c)** Gross primary productivity (GPP) and **d)** Leaf area index (LAI). The dashed color
777 lines represent the model runs with different vegetation cover products: GLC 2000 (purple),
778 NALCMS (blue), ESA CCI (light blue), and the Hybrid-9PFT (green). The additional color lines
779 denote various reference data sets. NFI and FOSXue are point-based reference data sets and are
780 therefore not displayed in panel a. Average AGB for FosXue is 6.0 kg C m^{-2} f and average AGB
781 for NFI is 4.6 kg C m^{-2}.

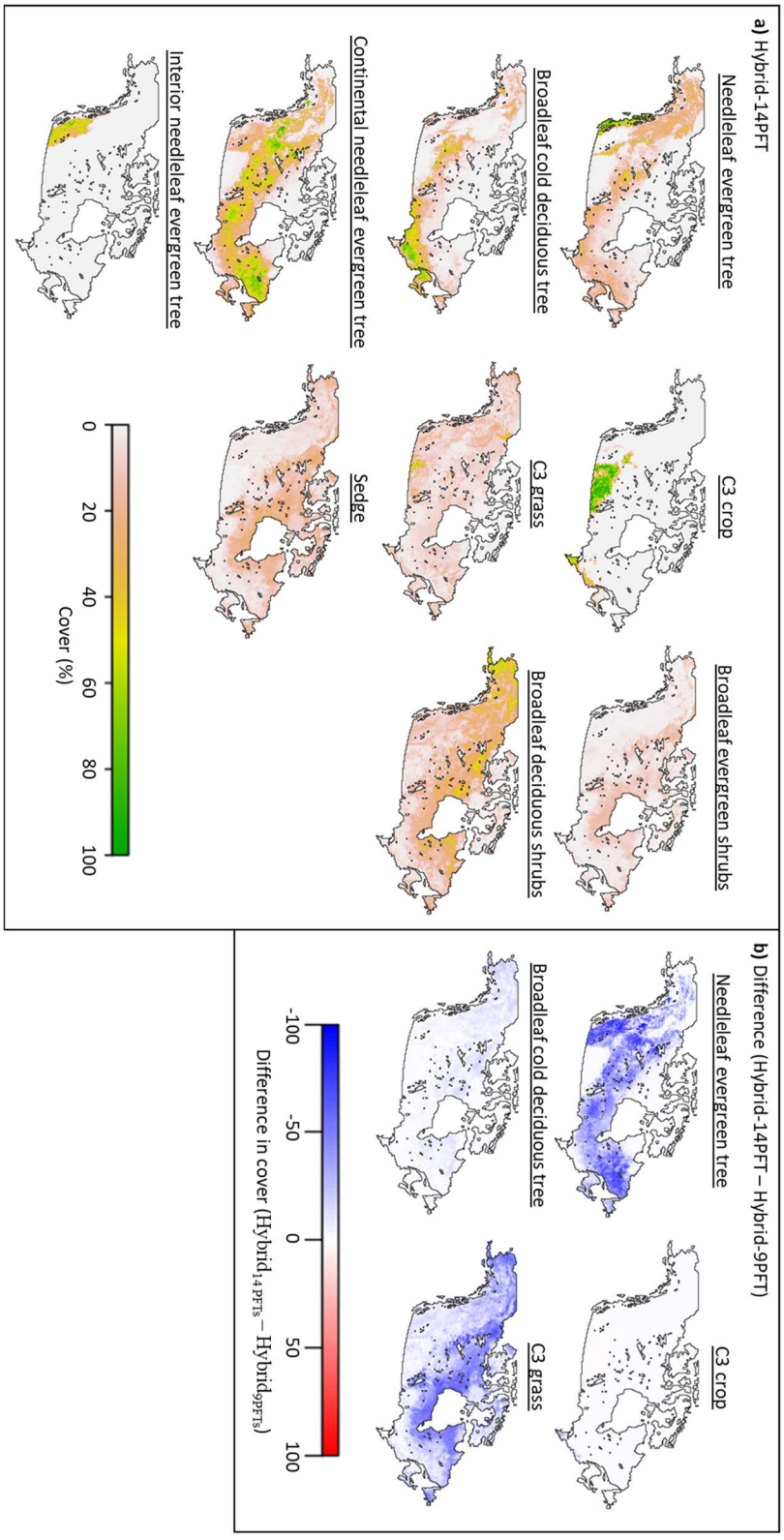

Figure 4: a) Maps of major plant function type (PFT) cover across Canada for the Hybrid-14PFT vegetation cover. **b)** Maps of the difference in PFT cover across Canada (Hybrid-14PFT – Hybrid-9PFT) for major PFTs present in both data sets.

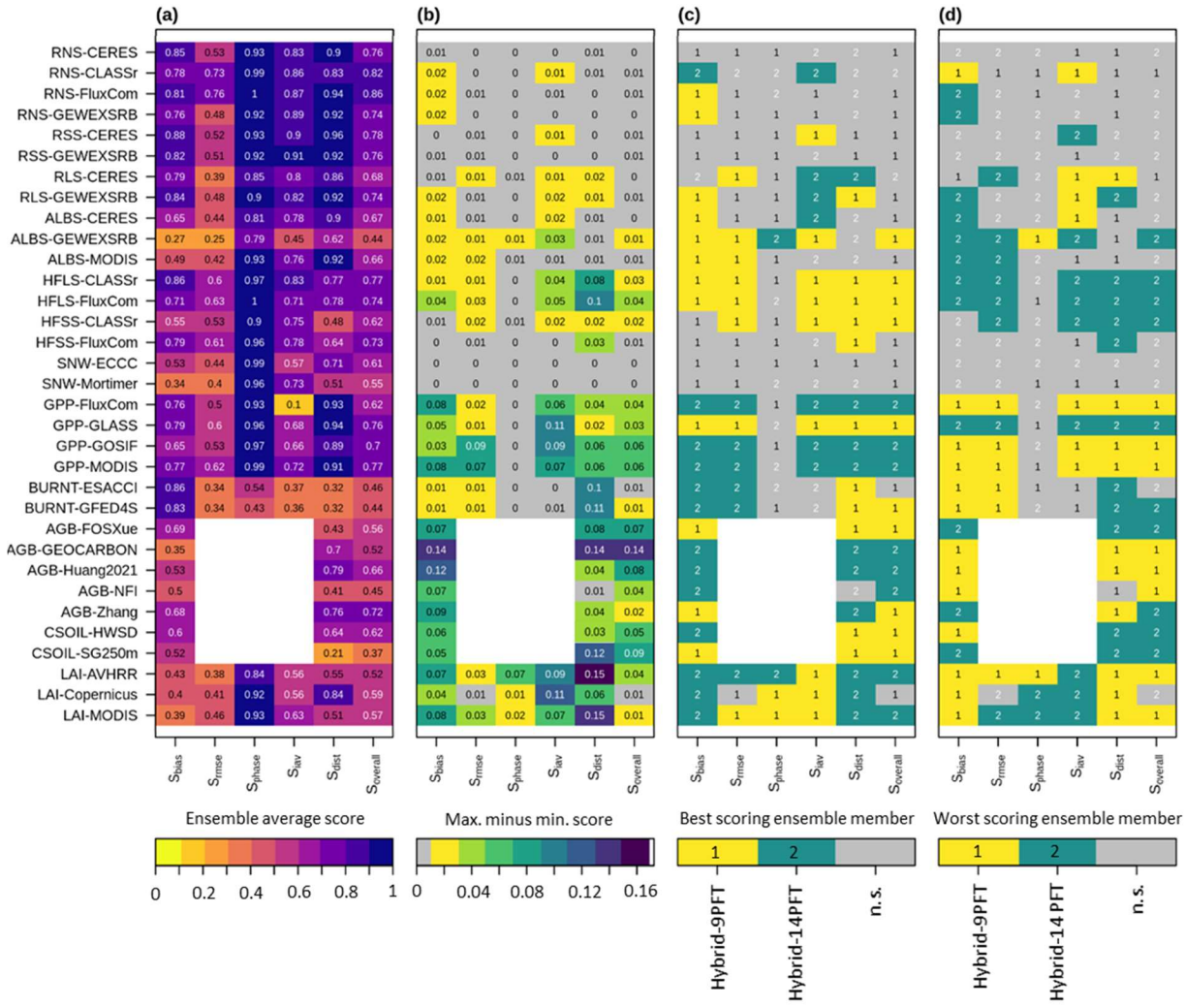

Figure 5: a) Mean ensemble score, **b)** maximum score difference among ensemble members, and ensemble members with the **c)** highest and **d)** lowest score for historical model runs using Hybrid-9PFT (1) and Hybrid-14PFT (2). Comparisons are grayed out in panels b-d when the difference between the maximum and minimum scores is less than 0.01.

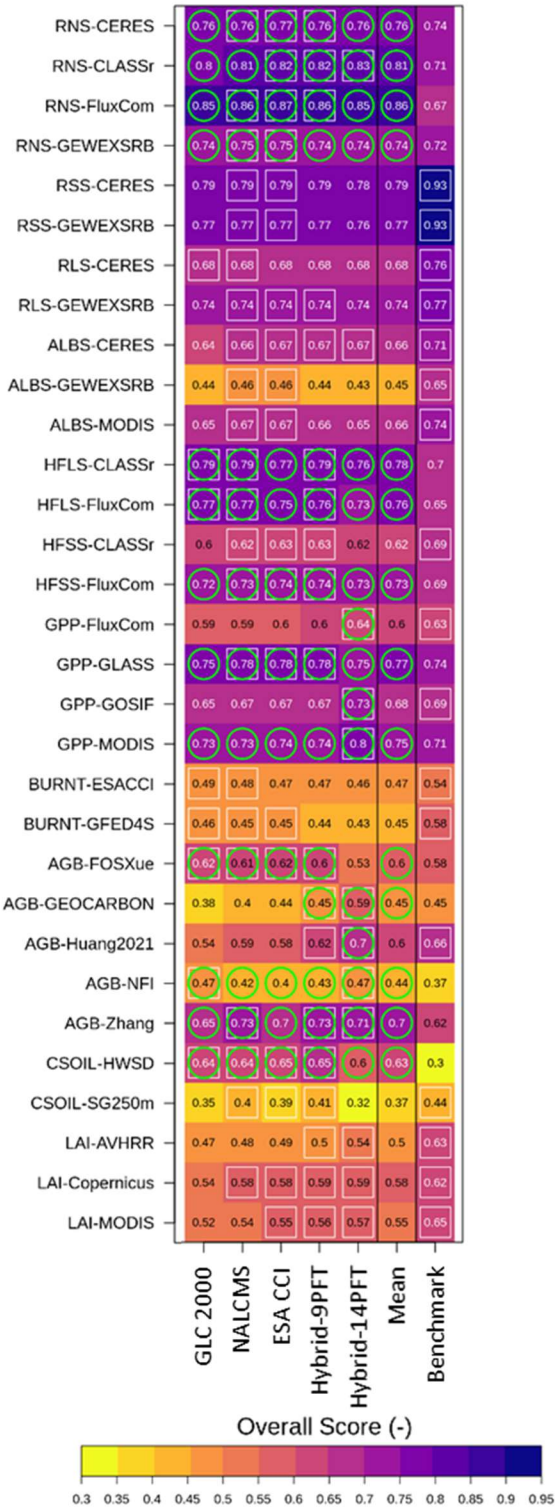

Figure 6: Overall model scores with benchmarks. Green circles denote model scores that meet or exceed the benchmark scores and white squares denote model scores that meet or exceed the multi-model mean.

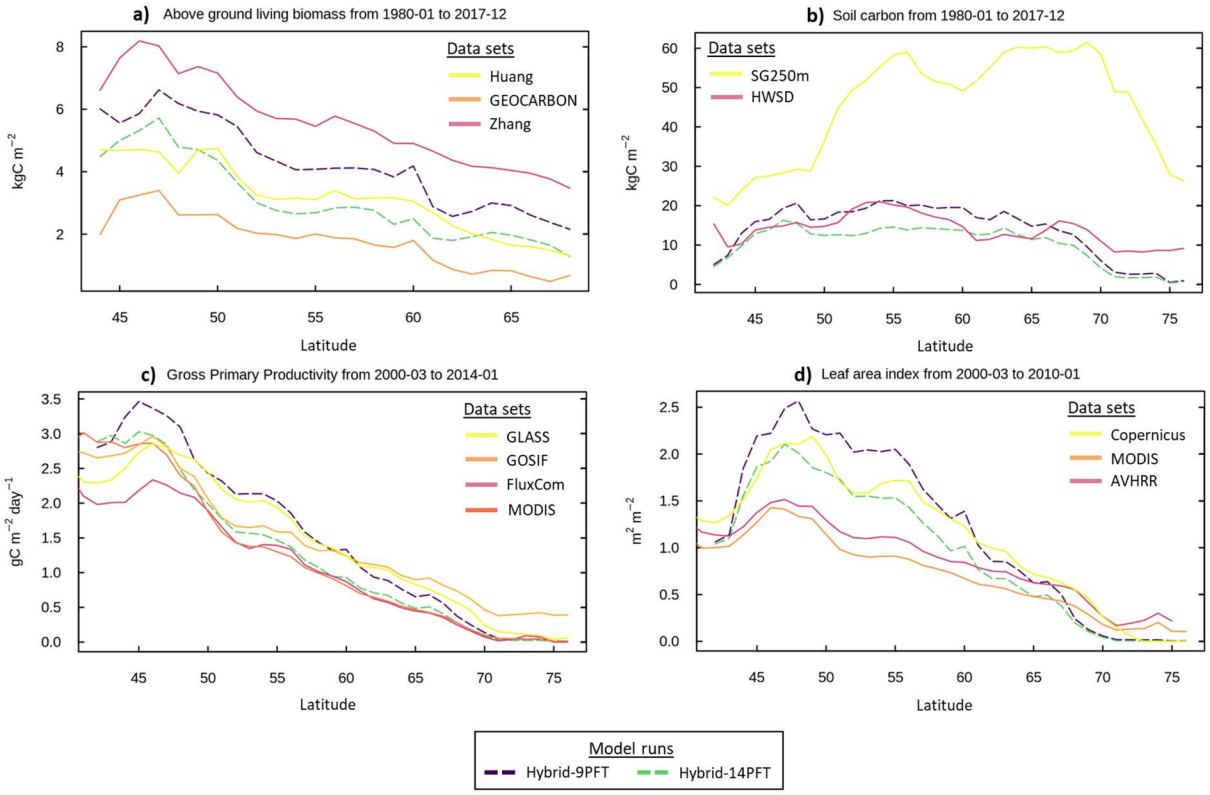

Figure 7: Plot of the average **a)** Above ground living biomass (AGB) **b)** Soil carbon (CSOIL) **c)** Gross primary productivity (GPP) and **d)** Leaf area index (LAI) across latitude. The dashed color lines represent the model runs with different vegetation cover products: Hybrid-9PFT (purple) and Hybrid-14PFT (green). The additional color lines denote various reference data sets. NFI and FOSXue are point-based reference data sets and are therefore not displayed in panel a.

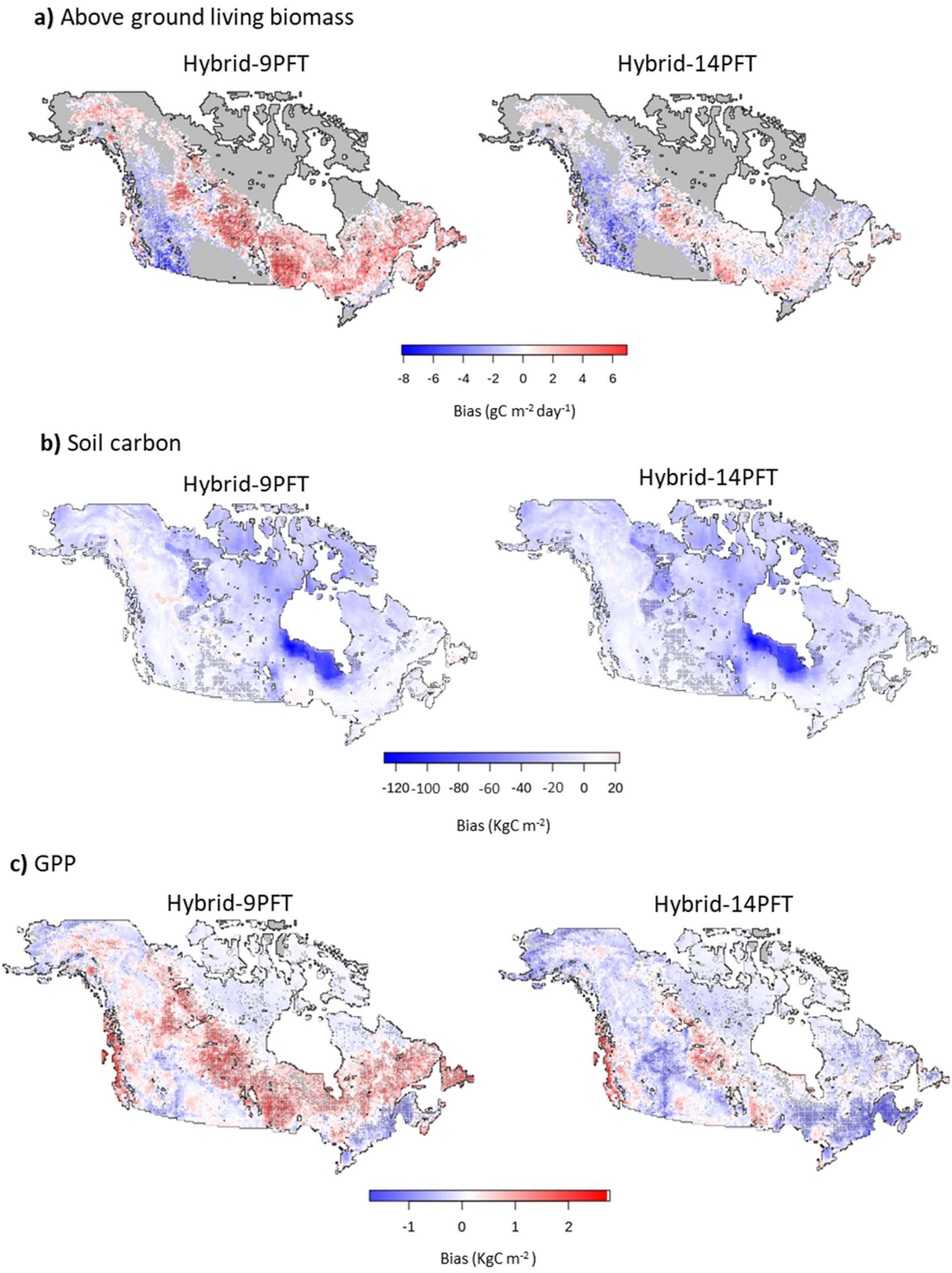
a) Above ground living biomass
Hybrid-9PFT
Hybrid-14PFT
-8 -6 -4 -2 0 2 4 6
Bias (gC m-2 day-1)
b) Soil carbon
Hybrid-9PFT
Hybrid-14PFT
-120 -100 -80 -60 -40 -20 0 20
Bias (KgC m-2)
c) GPP
Hybrid-9PFT
Hybrid-14PFT
-1 0 1 2
Bias (KgC m-2)

804

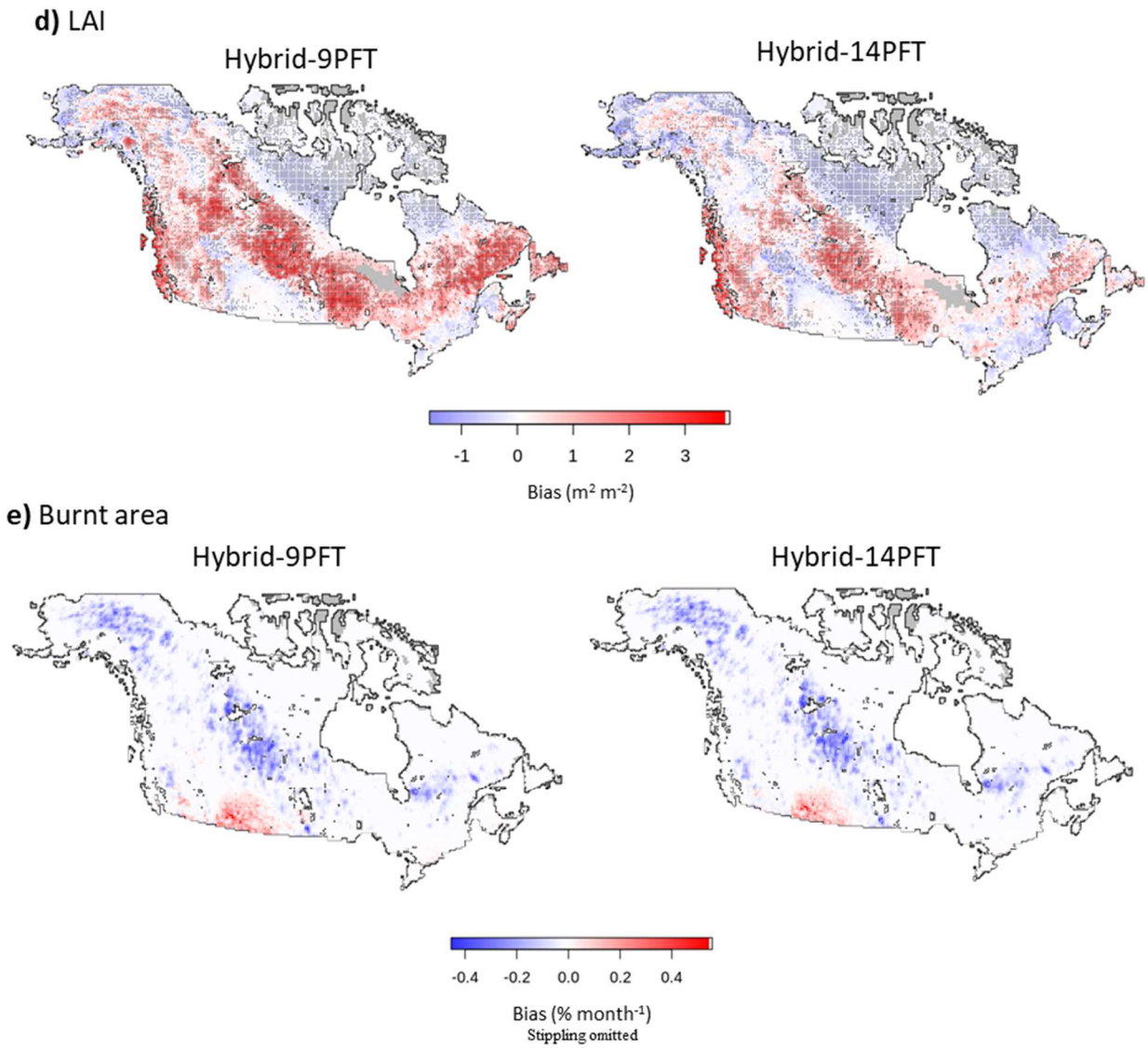

Figure 8: Average bias for **a)** Above ground living biomass (AGB), **b)** Soil carbon (CSOIL), **c)** Gross primary productivity, **d)** Leaf area index (LAI), and **e)** burnt area (BURNT), for CLASSIC using the Hybrid-9PFT and Hybrid-14PFT, versus gridded reference data sets (Table 2, Section 2.5). Stippling denotes areas where the model falls outside the 95% confidence interval for reference data sets. Gray cells denote land areas not covered by one or more of the reference data sets. The 9 PFT model run and stippling have been omitted in panel e because of the strength and similarity of the biases. NFI and FOSXue are point-based reference data sets and are therefore not included in panel a.

10. Tables

Table 1: Plant functional types used by CLASSIC in the default 9 PFT configuration as compared to 14 PFT configuration tested in our study. The mapping between CLASS and CTEM PFTs is shown along with the parameters for the maximum rate of carboxylation by Rubisco (v_{max} ; µmol CO_2 m^{-2} s^{-1}), maximum cold stress leaf loss rate ($\Omega_{C,max}$; day^{-1}), and the maximum drought stress leaf loss rate ($\Omega_{D,max}$; day^{-1}).

CLASS PFTs	CTEM PFTs	Configuration	v_{max}	$\Omega_{C,max}$	$\Omega_{D,max}$	references
Needleleaf tree	Needleleaf Evergreen tree	**9 PFT**	42	0.1	0.0025	Melton and Arora 2016
	Needleleaf Deciduous tree	**9 PFT**	42	0.2	0.005	Melton and Arora 2016
	Continental Needleleaf Evergreen tree	14 PFT	24.5	0.1	0.0025	Qu et al., 2021
	Interior Needleleaf Evergreen tree	14 PFT	42	0.05	0.00125	Peng et al., 2014
Broadleaf tree	Broadleaf Evergreen tree	**9 PFT**	35	0.3	0.005	Melton and Arora 2016
	Broadleaf Cold Deciduous tree	**9 PFT**	57	0.3	0.005	Melton and Arora 2016
	Broadleaf Drought/Dry Deciduous tree	**9 PFT**	40	0.15	0.025	Melton and Arora 2016
Crop	C3 Crop	**9 PFT**	55	0.15	0.005	Melton and Arora 2016
	C4 Crop	9 PFT	40	0.15	0.005	Melton and Arora 2016
Grass	C3 Grass	**9 PFT**	55	0.15	0.05	Melton and Arora 2016
	C4 Grass	**9 PFT**	15	0.15	0.05	Melton and Arora 2016
	Sedge[1]	14 PFT	40	0.15	0.05	Meyer et al., 2021
Broadleaf shrub	Broadleaf evergreen Shrubs[1]	14 PFT	60	0.1	0.0025	Meyer et al., 2021
	Broadleaf deciduous Shrubs[1]	14 PFT	60	0.2	0.005	Meyer et al., 2021

[1]See Meyer et al., 2021 for additional details regarding the sedge and shrubs PFTs and associated parameters.

824 **Table 2:** Overview of the reference data sets used in our model evaluation. The acronyms given
825 here are defined in section 2.5.

Data set	Variables	Method	Period	References
FluxCom	GPP, RNS, HFLS, HFSS	Machine learning ensemble	1980 - 2013	Jung et al., 2019
MODIS	ALBS,	BDRF,	2000 - 2014,	Strahler et al., 1999;
	GPP,	Light use efficiency model,	2000 - 2016,	Zhang et al., 2017;
	LAI	Radiative transfer model	2000 - 2018	Myneni et al., 2002
GOSIF	GPP	Statistical model	2000 - 2018	Li & Xiao, 2019
GLASS	GPP	Light use efficiency model	1982 - 2018	Liang et al., 2021
AVHRR	LAI	Neural network	1982 - 2010	Claverie et al., 2016
Copernicus	LAI	Neural network	1999 - 2020	Verger et al., 2016
GFED4S	BURNT	burned-area mapping	2001 - 2015	Giglio et al., 2013
ESACCI	BURNT	Burned area mapping	2001 - 2019	Chuvieco et al., 2018
GEOCARBON	AGB	Machine learning	snapshot	Avitabile et al., 2016; Santoro et al., 2015
Zhang	AGB	Data fusion	snapshot	Zhang et al., 2020
FOSXue	AGB	in situ measurment	1999 - 2018	Schepaschenko et al., 2019; Xue et al., 2017
NFI	AGB	in situ measurment	2008 - 2017	Gillis et al., 2005
Huang2021	AGB	Remote sensed SAR	snapshot	Haung et al., 2021
HWSD	CSOIL	Soil inventory	snapshot	Todd-Brown et al., 2013
SG250m	CSOIL	Machine learning ensemble	snapshot	Hengl et al., 2017
CERES	ALBS,RSS,RLS,RNS	Radiative transfer model	2000 - 2013	Kato et al., 2013
GEWEXSRB	ALBS, RSS, RLS, RNS	Radiative transfer model	1984 - 2007	Zhang et al., 2011
CLASSr	RNS, HFLS, HFSS	Blended product	2003 - 2009	Hobeichi et al., 2020
ECCC	SNW	Blended product	1981 - 2018	Brown et al., 2003; Brun et al., 2013; Takala et al., 2011; Gelaro et al., 2017
Mortimer	SNW	In situ measurments	1970 - 2017	Mortimer et al., 2020

826

11. References

Anderegg, L. D. L., Griffith, D. M., Cavender-Bares, J., Riley, W. J., Berry, J. A., Dawson, T. E., & Still, C. J. (2022). Representing plant diversity in land models: An evolutionary approach to make "Functional Types" more functional. *Global Change Biology*, *28*(8), 2541–2554.

Arora, V. K. (2003). Simulating energy and carbon fluxes over winter wheat using coupled land surface and terrestrial ecosystem models. *Agricultural and Forest Meteorology*, *118*(1), 21–47.

Arora, V. K., & Boer, G. J. (2010). Uncertainties in the 20th century carbon budget associated with land use change. *Global Change Biology*, *16*(12), 3327–3348.

Arora, V. K., Boer, G. J., Christian, J. R., Curry, C. L., Denman, K. L., Zahariev, K., Flato, G. M., Scinocca, J. F., Merryfield, W. J., & Lee, W. G. (2009). The Effect of Terrestrial Photosynthesis Down Regulation on the Twentieth-Century Carbon Budget Simulated with the CCCma Earth System Model. *Journal of Climate*, *22*(22), 6066–6088.

Arora, V. K., & Melton, J. R. (2018). Reduction in global area burned and wildfire emissions since 1930s enhances carbon uptake by land. *Nature Communications*, *9*(1), 1326.

Asaadi, A., & Arora, V. K. (2021). Implementation of nitrogen cycle in the CLASSIC land model. *Biogeosciences* , *18*(2), 669–706.

Asaadi, Arora, Melton, & Bartlett. (2018). An improved parameterization of leaf area index (LAI) seasonality in the Canadian Land Surface Scheme (CLASS) and Canadian Terrestrial Ecosystem …. *Biogeosciences* . https://bg.copernicus.org/articles/15/6885/2018/

Avitabile, V., Herold, M., Heuvelink, G. B. M., Lewis, S. L., Phillips, O. L., Asner, G. P., Armston, J., Ashton, P. S., Banin, L., Bayol, N., Berry, N. J., Boeckx, P., de Jong, B. H. J.,

DeVries, B., Girardin, C. A. J., Kearsley, E., Lindsell, J. A., Lopez-Gonzalez, G., Lucas, R., … Willcock, S. (2016). An integrated pan-tropical biomass map using multiple reference datasets. *Global Change Biology*, *22*(4), 1406–1420.

Babst, F., Bouriaud, O., Poulter, B., Trouet, V., Girardin, M. P., & Frank, D. C. (2019). Twentieth century redistribution in climatic drivers of global tree growth. *Science Advances*, *5*(1), eaat4313.

Baret, F., Morissette, J. T., Fernandes, R. A., Champeaux, J. L., Myneni, R. B., Chen, J., Plummer, S., Weiss, M., Bacour, C., Garrigues, S., & Nickeson, J. E. (2006). Evaluation of the representativeness of networks of sites for the global validation and intercomparison of land biophysical products: proposition of the CEOS-BELMANIP. *IEEE Transactions on Geoscience and Remote Sensing: A Publication of the IEEE Geoscience and Remote Sensing Society*, *44*(7), 1794–1803.

Bartholomé, E., & Belward, A. S. (2005). GLC2000: a new approach to global land cover mapping from Earth observation data. *International Journal of Remote Sensing*, *26*(9), 1959–1977.

Beaudoin, A., Bernier, P. Y., Villemaire, P., Guindon, L., & Guo, X. J. (2018). Tracking forest attributes across Canada between 2001 and 2011 using a k nearest neighbors mapping approach applied to MODIS imagery. *Canadian Journal of Forest Research. Journal Canadien de La Recherche Forestiere*, *48*(1), 85–93.

Berner, L. T., Massey, R., Jantz, P., Forbes, B. C., Macias-Fauria, M., Myers-Smith, I., Kumpula, T., Gauthier, G., Andreu-Hayles, L., Gaglioti, B. V., Burns, P., Zetterberg, P., D'Arrigo, R., & Goetz, S. J. (2020). Summer warming explains widespread but not uniform greening in the Arctic tundra biome. *Nature Communications*, *11*(1), 4621.

873 Bonan, G. B., Levis, S., Kergoat, L., & Oleson, K. W. (2002). Landscapes as patches of plant
874 functional types: An integrating concept for climate and ecosystem models. *Global*
875 *Biogeochemical Cycles*, *16*(2), 5–1 – 5–23.
876 Box, E. O. (1996). Plant functional types and climate at the global scale. *Journal of Vegetation*
877 *Science: Official Organ of the International Association for Vegetation Science*, *7*(3), 309–
878 320.
879 Box, J. E., Colgan, W. T., Christensen, T. R., Schmidt, N. M., Lund, M., Parmentier, F.-J. W.,
880 Brown, R., Bhatt, U. S., Euskirchen, E. S., Romanovsky, V. E., Walsh, J. E., Overland, J.
881 E., Wang, M., Corell, R. W., Meier, W. N., Wouters, B., Mernild, S., Mård, J., Pawlak, J.,
882 & Olsen, M. S. (2019). Key indicators of Arctic climate change: 1971–2017. *Environmental*
883 *Research Letters: ERL [Web Site]*, *14*(4), 045010.
884 Brown, R. D., Brasnett, B., & Robinson, D. (2003). Gridded North American monthly snow
885 depth and snow water equivalent for GCM evaluation. *Atmosphere-Ocean*, *41*(1), 1–14.
886 Brun, E., Vionnet, V., Boone, A., Decharme, B., Peings, Y., Valette, R., Karbou, F., & Morin, S.
887 (2013). Simulation of Northern Eurasian Local Snow Depth, Mass, and Density Using a
888 Detailed Snowpack Model and Meteorological Reanalyses. *Journal of Hydrometeorology*,
889 *14*(1), 203–219.
890 CCFM: National Forestry Database. (2022). *Area of moderate to severe defoliation (including*
891 *beetle-killed trees) by insects*. http://nfdp.ccfm.org/en/data/insects.php
892 Cecil, Buechler, & Blakeslee. (2014). LIS/OTD Gridded Lightning Climatology Data Sets. .
893 *gov/pub/lis/climatology/LIS-OTD/HRFC/] from the …*.
894 Chaste, E., Girardin, M. P., Kaplan, J. O., Portier, J., Bergeron, Y., & Hély, C. (2017). The
895 pyrogeography of eastern boreal Canada from 1901 to 2012 simulated with the LPJ-LMfire

model. *Biogeosciences Discussions* , 1–33.

Chen, J., Chen, W., Liu, J., Cihlar, J., & Gray, S. (2000). Annual carbon balance of Canada's forests during 1895-1996. *Global Biogeochemical Cycles*, *14*(3), 839–849.

Chen, J. M., Ju, W., Cihlar, J., Price, D., Liu, J., Chen, W., Pan, J., Black, A., & Barr, A. (2003). Spatial distribution of carbon sources and sinks in Canada's forests. *Tellus. Series B, Chemical and Physical Meteorology*, *55*(2), 622–641.

Chini, L., Hurtt, G., Sahajpal, R., Frolking, S., Klein Goldewijk, K., Sitch, S., Ganzenmüller, R., Ma, L., Ott, L., Pongratz, J., & Poulter, B. (2021). Land-use harmonization datasets for annual global carbon budgets. *Earth System Science Data*, *13*(8), 4175–4189.

Chuvieco, E., Lizundia-Loiola, J., Pettinari, M. L., Ramo, R., Padilla, M., Tansey, K., Mouillot, F., Laurent, P., Storm, T., Heil, A., & Plummer, S. (2018). Generation and analysis of a new global burned area product based on MODIS 250 m reflectance bands and thermal anomalies. *Earth System Science Data Discussions*, 1–24.

Claverie, M., Matthews, J. L., Vermote, E. F., & Justice, C. O. (2016). A 30+ Year AVHRR LAI and FAPAR Climate Data Record: Algorithm Description and Validation. *Remote Sensing*, *8*(3), 263.

Curasi, S. R., Fetcher, N., Hewitt, R. E., Lafleur, P. M., Loranty, M. M., Mack, M. C., May, J. L., Myers-Smith, I. H., Natali, S. M., Oberbauer, S. F., Parker, T. C., Sonnentag, O., Vargas Zesati, S. A., Wullschleger, S. D., & Rocha, A. V. (2022). Range shifts in a foundation sedge potentially induce large Arctic ecosystem carbon losses and gains. *Environmental Research Letters: ERL [Web Site]*, *17*(4), 045024.

D'Orangeville, L., Houle, D., Duchesne, L., Phillips, R. P., Bergeron, Y., & Kneeshaw, D. (2018). Beneficial effects of climate warming on boreal tree growth may be transitory.

Nature Communications, *9*(1), 3213.

ECMWF. (2019). *ERA5 reanalysis (0.25 degree latitude-longitude grid)*. Research Data Archive at the National Center for Atmospheric Research ….

Epstein, H. E., Chapin, F. S., III, Walker, M. D., & Starfield, A. M. (2001). Analyzing the functional type concept in arctic plants using a dynamic vegetation model. *Oikos* , *95*(2), 239–252.

European Space Agency. (2017). *Land Cover CCI Product User Guide Version 2 Tech. Rep*.

Fisher, J. B., Hayes, D. J., Schwalm, C. R., Huntzinger, D. N., Stofferahn, E., Schaefer, K., Luo, Y., Wullschleger, S. D., Goetz, S., Miller, C. E., Griffith, P., Chadburn, S., Chatterjee, A., Ciais, P., Douglas, T. A., Genet, H., Ito, A., Neigh, C. S. R., Poulter, B., … Zhang, Z. (2018). Missing pieces to modeling the Arctic-Boreal puzzle. *Environmental Research Letters: ERL [Web Site]*, *13*(2), 020202.

Friedlingstein, P., Jones, M. W., O'Sullivan, M., Andrew, R. M., Bakker, D. C. E., Hauck, J., Le Quéré, C., Peters, G. P., Peters, W., Pongratz, J., & Others. (2022). Global carbon budget 2021. *Earth System Science Data*, *14*(4), 1917–2005.

Friedlingstein, P., Jones, M. W., O'Sullivan, M., Andrew, R. M., Hauck, J., Peters, G. P., Peters, W., Pongratz, J., Sitch, S., Le Quéré, C., & Others. (2019). *Global Carbon Budget 2019, Earth Syst. Sci. Data, 11, 1783--1838*.

Fritz, S., See, L., McCallum, I., Schill, C., Obersteiner, M., van der Velde, M., Boettcher, H., Havlík, P., & Achard, F. (2011). Highlighting continued uncertainty in global land cover maps for the user community. *Environmental Research Letters: ERL [Web Site]*, *6*(4), 044005.

Gelaro, R., McCarty, W., Suárez, M. J., Todling, R., Molod, A., Takacs, L., Randles, C.,

Darmenov, A., Bosilovich, M. G., Reichle, R., Wargan, K., Coy, L., Cullather, R., Draper, C., Akella, S., Buchard, V., Conaty, A., da Silva, A., Gu, W., … Zhao, B. (2017). The Modern-Era Retrospective Analysis for Research and Applications, Version 2 (MERRA-2). *Journal of Climate*, *30*(Iss 13), 5419–5454.

Giglio, L., Randerson, J. T., & van der Werf, G. R. (2013). Analysis of daily, monthly, and annual burned area using the fourth-generation global fire emissions database (GFED4). *Journal of Geophysical Research. Biogeosciences*, *118*(1), 317–328.

Giles-Hansen, K., & Wei, X. (2022). Cumulative disturbance converts regional forests into a substantial carbon source. *Environmental Research Letters: ERL [Web Site]*, *17*(4), 044049.

Gillis, M. D., Omule, A. Y., & Brierley, T. (2005). Monitoring Canada's forests: The National Forest Inventory. *Forestry Chronicle*, *81*(2), 214–221.

Girardin, M. P., Bouriaud, O., Hogg, E. H., Kurz, W., Zimmermann, N. E., Metsaranta, J. M., de Jong, R., Frank, D. C., Esper, J., Büntgen, U., Guo, X. J., & Bhatti, J. (2016). No growth stimulation of Canada's boreal forest under half-century of combined warming and CO2 fertilization. *Proceedings of the National Academy of Sciences of the United States of America*, *113*(52), E8406–E8414.

Gou, J., Wang, F., Jin, K., Mu, X., & Chen, D. (2019). More realistic land-use and vegetation parameters in a regional climate model reduce model biases over China. *International Journal of Climatology*, *39*(12), 4825–4837.

Government of Canada. (2016). *Pan-canadian framework on clean growth and climate change*.

Harper, Wiltshire, & Cox. (2018). Vegetation distribution and terrestrial carbon cycle in a carbon cycle configuration of JULES4. 6 with new plant functional types. *Geoscientific Model Development*. https://gmd.copernicus.org/articles/11/2857/2018/

965 Hartley, A. J., MacBean, N., Georgievski, G., & Bontemps, S. (2017). Uncertainty in plant
966 functional type distributions and its impact on land surface models. *Remote Sensing of*
967 *Environment*, *203*, 71–89.
968 Hayes, D. J., Turner, D. P., Stinson, G., McGuire, A. D., Wei, Y., West, T. O., Heath, L. S.,
969 Jong, B., McConkey, B. G., Birdsey, R. A., Kurz, W. A., Jacobson, A. R., Huntzinger, D.
970 N., Pan, Y., Post, W. M., & Cook, R. B. (2012). Reconciling estimates of the contemporary
971 North American carbon balance among terrestrial biosphere models, atmospheric
972 inversions, and a new approach for estimating net ecosystem exchange from inventory-
973 based data. *Global Change Biology*, *18*(4), 1282–1299.
974 Hengl, T., Mendes de Jesus, J., Heuvelink, G. B. M., Ruiperez Gonzalez, M., Kilibarda, M.,
975 Blagotić, A., Shangguan, W., Wright, M. N., Geng, X., Bauer-Marschallinger, B., Guevara,
976 M. A., Vargas, R., MacMillan, R. A., Batjes, N. H., Leenaars, J. G. B., Ribeiro, E.,
977 Wheeler, I., Mantel, S., & Kempen, B. (2017). SoilGrids250m: Global gridded soil
978 information based on machine learning. *PloS One*, *12*(2), e0169748.
979 Hermosilla, T., Wulder, M. A., White, J. C., Coops, N. C., & Hobart, G. W. (2018). Disturbance-
980 Informed Annual Land Cover Classification Maps of Canada's Forested Ecosystems for a
981 29-Year Landsat Time Series. *Canadian Journal of Remote Sensing*, *44*(1), 67–87.
982 Hobeichi, S., Abramowitz, G., & Evans, J. (2020). Conserving Land–Atmosphere Synthesis
983 Suite (CLASS). *Journal of Climate*, *33*(5), 1821–1844.
984 Huang, Y., Ciais, P., Santoro, M., Makowski, D., Chave, J., Schepaschenko, D., Abramoff, R. Z.,
985 Goll, D. S., Yang, H., Chen, Y., Wei, W., & Piao, S. (2021). A global map of root biomass
986 across the world's forests. *Earth System Science Data*, *13*(9), 4263–4274.
987 Huntzinger, D. N., Post, W. M., Wei, Y., Michalak, A. M., West, T. O., Jacobson, A. R., Baker,

I. T., Chen, J. M., Davis, K. J., Hayes, D. J., Hoffman, F. M., Jain, A. K., Liu, S., McGuire, A. D., Neilson, R. P., Potter, C., Poulter, B., Price, D., Raczka, B. M., … Cook, R. (2012). North American Carbon Program (NACP) regional interim synthesis: Terrestrial biospheric model intercomparison. *Ecological Modelling*, *232*, 144–157.

Iversen, C. M., & McCormack, M. L. (2021). Filling gaps in our understanding of belowground plant traits across the world: an introduction to a Virtual Issue. *The New Phytologist*, *231*(6), 2097–2103.

Iversen, C. M., McCormack, M. L., Powell, A. S., Blackwood, C. B., Freschet, G. T., Kattge, J., Roumet, C., Stover, D. B., Soudzilovskaia, N. A., Valverde-Barrantes, O. J., Bodegom, P. M., & Violle, C. (2017). A global Fine-Root Ecology Database to address below-ground challenges in plant ecology. *The New Phytologist*, *215*(1), 15–26.

Jia, G. J., Epstein, H. E., & Walker, D. A. (2003). Greening of arctic Alaska, 1981–2001. *Geophysical Research Letters*, *30*(20). https://doi.org/10.1029/2003gl018268

Jia, G. J., Epstein, H. E., & Walker, D. A. (2009). Vegetation greening in the Canadian Arctic related to decadal warming. *Journal of Environmental Monitoring: JEM*, *11*(12), 2231–2238.

Jung, M., Koirala, S., Weber, U., Ichii, K., Gans, F., Camps-Valls, G., Papale, D., Schwalm, C., Tramontana, G., & Reichstein, M. (2019). The FLUXCOM ensemble of global land-atmosphere energy fluxes. *Scientific Data*, *6*(1), 74.

Jung, M., Schwalm, C., Migliavacca, M., Walther, S., Camps-Valls, G., Koirala, S., Anthoni, P., Besnard, S., Bodesheim, P., Carvalhais, N., Chevallier, F., Gans, F., Goll, D. S., Haverd, V., Köhler, P., Ichii, K., Jain, A. K., Liu, J., Lombardozzi, D., … Reichstein, M. (2020). Scaling carbon fluxes from eddy covariance sites to globe: synthesis and evaluation of the

FLUXCOM approach. *Biogeosciences* , *17*(5), 1343–1365.

Jung, M., Vetter, M., Herold, M., Churkina, G., Reichstein, M., Zaehle, S., Ciais, P., Viovy, N., Bondeau, A., Chen, Y., Trusilova, K., Feser, F., & Heimann, M. (2007). Uncertainties of modeling gross primary productivity over Europe: A systematic study on the effects of using different drivers and terrestrial biosphere models. *Global Biogeochemical Cycles*, *21*(4). https://doi.org/10.1029/2006gb002915

Ju, W., & Chen, J. M. (2008). Simulating the effects of past changes in climate, atmospheric composition, and fire disturbance on soil carbon in Canada's forests and wetlands. *Global Biogeochemical Cycles*, *22*(3). https://doi.org/10.1029/2007GB002935

Kato, S., Loeb, N. G., Rose, F. G., Doelling, D. R., Rutan, D. A., Caldwell, T. E., Yu, L., & Weller, R. A. (2013). Surface Irradiances Consistent with CERES-Derived Top-of-Atmosphere Shortwave and Longwave Irradiances. *Journal of Climate*, *26*(9), 2719–2740.

Kattge, J., Bönisch, G., Díaz, S., Lavorel, S., Prentice, I. C., Leadley, P., Tautenhahn, S., Werner, G. D. A., Aakala, T., Abedi, M., Acosta, A. T. R., Adamidis, G. C., Adamson, K., Aiba, M., Albert, C. H., Alcántara, J. M., Alcázar C, C., Aleixo, I., Ali, H., … Wirth, C. (2020). TRY plant trait database - enhanced coverage and open access. *Global Change Biology*, *26*(1), 119–188.

Keenan, T. F., & Williams, C. A. (2018). The Terrestrial Carbon Sink. *Annual Review of Environment and Resources*, *43*(1), 219–243.

Kim. (2017). Global soil wetness project phase 3 atmospheric boundary conditions (Experiment 1). *Data Integration and Analysis System (DIAS), Data Set*.

Koca, D., Smith, B., & Sykes, M. T. (2006). Modelling Regional Climate Change Effects On Potential Natural Ecosystems in Sweden. *Climatic Change*, *78*(2), 381–406.

Kuntoro, Wahyu, & Yamashita. (2009). The Effect of Deforestation on Regional Terrestrial Carbon Balance: A Case Study of Kalimantan Island. *The Journal of International Advanced Otology*. https://cir.nii.ac.jp/crid/1390290699831320064

Kurz, W. A., Dymond, C. C., Stinson, G., Rampley, G. J., Neilson, E. T., Carroll, A. L., Ebata, T., & Safranyik, L. (2008). Mountain pine beetle and forest carbon feedback to climate change. *Nature*, *452*(7190), 987–990.

Kurz, W. A., Dymond, C. C., White, T. M., Stinson, G., Shaw, C. H., Rampley, G. J., Smyth, C., Simpson, B. N., Neilson, E. T., Trofymow, J. A., Metsaranta, J., & Apps, M. J. (2009). CBM-CFS3: A model of carbon-dynamics in forestry and land-use change implementing IPCC standards. *Ecological Modelling*, *220*(4), 480–504.

Kyker-Snowman, E., Lombardozzi, D. L., Bonan, G. B., Cheng, S. J., Dukes, J. S., Frey, S. D., Jacobs, E. M., McNellis, R., Rady, J. M., Smith, N. G., Thomas, R. Q., Wieder, W. R., & Grandy, A. S. (2021). Increasing the spatial and temporal impact of ecological research: A roadmap for integrating a novel terrestrial process into an Earth system model. *Global Change Biology*. https://doi.org/10.1111/gcb.15894

Land Cover v0.2. (2021). http://ckan.snap.uaf.edu/dataset/land-cover-v0-2

Landry, J.-S., Parrott, L., Price, D. T., Ramankutty, N., & Matthews, H. D. (2016). Modelling long-term impacts of mountain pine beetle outbreaks on merchantable biomass, ecosystem carbon, albedo, and radiative forcing. *Biogeosciences* , *13*(18), 5277–5295.

Lange, S. (2019). *WFDE5 over land merged with ERA5 over the ocean (W5E5). V. 1.0. GFZ Data Services*.

Lange, S. (2020a). *ISIMIP3BASD (Version 2.3)*. https://doi.org/10.5281/zenodo.3648654

Lange, S. (2020b). *The Inter-Sectoral Impact Model Intercomparison Project Input data set:*

GSWP3-W5E5. https://www. isimip.org/gettingstarted/input-data-bias-correction/details/80/

Latifovic, R., Pouliot, D., & Olthof, I. (2017). Circa 2010 Land Cover of Canada: Local Optimization Methodology and Product Development. *Remote Sensing*, *9*(11), 1098.

Lenton, T. M., Held, H., Kriegler, E., Hall, J. W., Lucht, W., Rahmstorf, S., & Schellnhuber, H. J. (2008). Tipping elements in the Earth's climate system. *Proceedings of the National Academy of Sciences of the United States of America*, *105*(6), 1786–1793.

Liang, S., Cheng, J., Jia, K., Jiang, B., Liu, Q., Xiao, Z., Yao, Y., Yuan, W., Zhang, X., Zhao, X., & Zhou, J. (2021). The Global Land Surface Satellite (GLASS) Product Suite. *Bulletin of the American Meteorological Society*, *102*(2), E323–E337.

Li, X., & Xiao, J. (2019). A Global, 0.05-Degree Product of Solar-Induced Chlorophyll Fluorescence Derived from OCO-2, MODIS, and Reanalysis Data. *Remote Sensing*, *11*(5), 517.

Lu, D., & Weng, Q. (2007). A survey of image classification methods and techniques for improving classification performance. *International Journal of Remote Sensing*, *28*(5), 823–870.

Macander, M. J., Nelson, P. R., Nawrocki, T. W., Frost, G. V., Orndahl, K. M., Palm, E. C., Wells, A. F., & Goetz, S. J. (2022). Time-series maps reveal widespread change in plant functional type cover across Arctic and boreal Alaska and Yukon. *Environmental Research Letters: ERL [Web Site]*, *17*(5), 054042.

MacKay, M. D., Meyer, G., & Melton, J. R. (2022). On the Discretization of Richards Equation in Canadian Land Surface Models. *Atmosphere-Ocean*, 1–11.

MacKenzie, W. H., & Meidinger, D. V. (2018). The Biogeoclimatic Ecosystem Classification Approach: an ecological framework for vegetation classification. *Phytocoenologia*, *48*(2),

203–213.

Marchand, Girardin, & Gauthier. (2018). Untangling methodological and scale considerations in growth and productivity trend estimates of Canada's forests. *Environmental Toxicology and Water Quality*. https://doi.org/10.1088/1748-9326/aad82a/meta

Ma, Z., Peng, C., Zhu, Q., Chen, H., Yu, G., Li, W., Zhou, X., Wang, W., & Zhang, W. (2012). Regional drought-induced reduction in the biomass carbon sink of Canada's boreal forests. *Proceedings of the National Academy of Sciences of the United States of America*, *109*(7), 2423–2427.

Mekonnen, Z. A., Riley, W. J., Berner, L. T., Bouskill, N. J., Torn, M. S., Iwahana, G., Breen, A. L., Myers-Smith, I. H., Criado, M. G., Liu, Y., Euskirchen, E. S., Goetz, S. J., Mack, M. C., & Grant, R. F. (2021). Arctic tundra shrubification: a review of mechanisms and impacts on ecosystem carbon balance. *Environmental Research Letters: ERL [Web Site]*, *16*(5), 053001.

Melton, J. R., & Arora, V. K. (2016). Competition between plant functional types in the Canadian Terrestrial Ecosystem Model (CTEM) v. 2.0. *Geoscientific Model Development*, *9*(1), 323–361.

Melton, J. R., Arora, V. K., Wisernig-Cojoc, E., Seiler, C., Fortier, M., Chan, E., & Teckentrup, L. (2020). CLASSIC v1. 0: the open-source community successor to the Canadian Land Surface Scheme (CLASS) and the Canadian Terrestrial Ecosystem Model (CTEM)–Part 1: Model framework and site-level performance. *Geoscientific Model Development*, *13*(6), 2825–2850.

Melton, J. R., Verseghy, D. L., Sospedra-Alfonso, R., & Gruber, S. (2019). Improving permafrost physics in the coupled Canadian Land Surface Scheme (v.3.6.2) and Canadian

Terrestrial Ecosystem Model (v.2.1) (CLASS-CTEM). *Geoscientific Model Development*, *12*(10), 4443–4467.

Meyer, G., Humphreys, E. R., Melton, J. R., Cannon, A. J., & Lafleur, P. M. (2021). Simulating shrubs and their energy and carbon dioxide fluxes in Canada's Low Arctic with the Canadian Land Surface Scheme Including Biogeochemical Cycles (CLASSIC). *Biogeosciences* , *18*(11), 3263–3283.

Miner, K. R., Turetsky, M. R., Malina, E., Bartsch, A., Tamminen, J., McGuire, A. D., Fix, A., Sweeney, C., Elder, C. D., & Miller, C. E. (2022). Permafrost carbon emissions in a changing Arctic. *Nature Reviews Earth & Environment*, *3*(1), 55–67.

Morales, P., Hickler, T., Rowell, D. P., Smith, B., & Sykes, M. T. (2007). Changes in European ecosystem productivity and carbon balance driven by regional climate model output. *Global Change Biology*, *13*(1), 108–122.

Mortimer, Mudryk, Derksen, & Luojus. (2020). Evaluation of long-term Northern Hemisphere snow water equivalent products. *Teaching in Higher Education*. https://tc.copernicus.org/articles/14/1579/2020/

Myers-Smith, I. H., Forbes, B. C., Wilmking, M., Hallinger, M., Lantz, T., Blok, D., Tape, K. D., Macias-Fauria, M., Sass-Klaassen, U., Lévesque, E., Boudreau, S., Ropars, P., Hermanutz, L., Trant, A., Collier, L. S., Weijers, S., Rozema, J., Rayback, S. A., Schmidt, N. M., … Hik, D. S. (2011). Shrub expansion in tundra ecosystems: dynamics, impacts and research priorities. *Environmental Research Letters: ERL [Web Site]*, *6*(4), 045509.

Myers-Smith, I. H., Kerby, J. T., Phoenix, G. K., Bjerke, J. W., Epstein, H. E., Assmann, J. J., John, C., Andreu-Hayles, L., Angers-Blondin, S., Beck, P. S. A., Berner, L. T., Bhatt, U. S., Bjorkman, A. D., Blok, D., Bryn, A., Christiansen, C. T., Cornelissen, J. H. C., Cunliffe, A.

M., Elmendorf, S. C., … Wipf, S. (2020). Complexity revealed in the greening of the Arctic. *Nature Climate Change*, *10*(2), 106–117.

Myneni, R. B., Hoffman, S., Knyazikhin, Y., Privette, J. L., Glassy, J., Tian, Y., Wang, Y., Song, X., Zhang, Y., Smith, G. R., Lotsch, A., Friedl, M., Morisette, J. T., Votava, P., Nemani, R. R., & Running, S. W. (2002). Global products of vegetation leaf area and fraction absorbed PAR from year one of MODIS data. *Remote Sensing of Environment*, *83*(1), 214–231.

Ottlé, C., Lescure, J., Maignan, F., Poulter, B., Wang, T., & Delbart, N. (2013). Use of various remote sensing land cover products for plant functional type mapping over Siberia. *Earth System Science Data*, *5*(2), 331–348.

Peng, Y., Arora, V. K., Kurz, W. A., Hember, R. A., Hawkins, B. J., Fyfe, J. C., & Werner, A. T. (2014). Climate and atmospheric drivers of historical terrestrial carbon uptake in the province of British Columbia, Canada. *Biogeosciences* , *11*(3), 635–649.

Potapov, P., Hansen, M. C., Stehman, S. V., Loveland, T. R., & Pittman, K. (2008). Combining MODIS and Landsat imagery to estimate and map boreal forest cover loss. *Remote Sensing of Environment*, *112*(9), 3708–3719.

Prentice, Liang, & Medlyn. (2015). Reliable, robust and realistic: the three R's of next-generation land-surface modelling. *Chemistry and Physics of Lipids*. https://acp.copernicus.org/articles/15/5987/2015/

Qiu, C., Zhu, D., Ciais, P., Guenet, B., & Peng, S. (2020). The role of northern peatlands in the global carbon cycle for the 21st century. *Global Ecology and Biogeography: A Journal of Macroecology*, *29*(5), 956–973.

Quaife, T., Quegan, S., Disney, M., Lewis, P., Lomas, M., & Woodward, F. I. (2008). Impact of land cover uncertainties on estimates of biospheric carbon fluxes. *Global Biogeochemical*

Cycles, *22*(4). https://doi.org/10.1029/2007gb003097

Qu, Roy, Melton, Black, & Amiro. (2021). Optimization of Maximum Photosynthetic Carboxylation Rate (Vc,max) in CLASSIC for North America's Boreal Forests using Eddy Covariance Data. *AGU Fall Meeting*. https://agu.confex.com/agu/fm21/meetingapp.cgi/Paper/915927

Reich, P. B., Bermudez, R., Montgomery, R. A., Rich, R. L., Rice, K. E., Hobbie, S. E., & Stefanski, A. (2022). Even modest climate change may lead to major transitions in boreal forests. *Nature*. https://doi.org/10.1038/s41586-022-05076-3

Reich, P. B., Koike, T., Gower, S. T., & Schoettle, A. W. (1995). 8 - Causes and Consequences of Variation in Conifer Leaf Life-Span. In W. K. Smith & T. M. Hinckley (Eds.), *Ecophysiology of Coniferous Forests* (pp. 225–254). Academic Press.

Reich, P. B., Sendall, K. M., Stefanski, A., Rich, R. L., Hobbie, S. E., & Montgomery, R. A. (2018). Effects of climate warming on photosynthesis in boreal tree species depend on soil moisture. *Nature*, *562*(7726), 263–267.

Rezende, L. F. C., Arenque, B. C., Aidar, S. T., Moura, M. S. B., Von Randow, C., Tourigny, E., Menezes, R. S. C., & Ometto, J. P. H. B. (2016). Is the maximum velocity of carboxylation (Vcmax) well adjusted for deciduous shrubs in DGVMs? A case study for the Caatinga biome in Brazil. *Modeling Earth Systems and Environment*, *2*(1), 42.

Rogers, A. (2014). The use and misuse of Vc,max in Earth System Models. *Photosynthesis Research*, *119*(1), 15–29.

Salkfield, Walton, & Mackenzie. (2016). Biogeoclimatic ecosystem classification map. *Ministry of Forests, Lands, Natural Resource*.

Santini, M., Collalti, A., & Valentini, R. (2014). Climate change impacts on vegetation and water

cycle in the Euro-Mediterranean region, studied by a likelihood approach. *Regional Environmental Change*, *14*(4), 1405–1418.

Santoro, M., Beaudoin, A., Beer, C., Cartus, O., Fransson, J. E. S., Hall, R. J., Pathe, C., Schmullius, C., Schepaschenko, D., Shvidenko, A., Thurner, M., & Wegmüller, U. (2015). Forest growing stock volume of the northern hemisphere: Spatially explicit estimates for 2010 derived from Envisat ASAR. *Remote Sensing of Environment*, *168*, 316–334.

Santoro, M., Cartus, O., Carvalhais, N., Rozendaal, D. M. A., Avitabile, V., Araza, A., de Bruin, S., Herold, M., Quegan, S., Rodríguez-Veiga, P., Balzter, H., Carreiras, J., Schepaschenko, D., Korets, M., Shimada, M., Itoh, T., Moreno Martínez, Á., Cavlovic, J., Cazzolla Gatti, R., … Willcock, S. (2021). The global forest above-ground biomass pool for 2010 estimated from high-resolution satellite observations. *Earth System Science Data*, *13*(8), 3927–3950.

Santoro, M., Cartus, O., Mermoz, S., Bouvet, A., Le Toan, T., Carvalhais, N., Rozendaal, D., Herold, M., Avitabile, V., Quegan, S., & Others. (2018). *GlobBiomass global above-ground biomass and growing stock volume datasets*. Technical Report. 2018. Available online: http://globbiomass. org/products ….

Schepaschenko, D., Chave, J., Phillips, O. L., Lewis, S. L., Davies, S. J., Réjou-Méchain, M., Sist, P., Scipal, K., Perger, C., Herault, B., Labrière, N., Hofhansl, F., Affum-Baffoe, K., Aleinikov, A., Alonso, A., Amani, C., Araujo-Murakami, A., Armston, J., Arroyo, L., … Zo-Bi, I. C. (2019). The Forest Observation System, building a global reference dataset for remote sensing of forest biomass. *Scientific Data*, *6*(1), 198.

Schulzweida, U., Kornblueh, L., & Quast, R. (2006). CDO user's guide. *Climate Data Operators, Version*, *1*(6), 205–209.

Schuur, E. A. G., & Mack, M. C. (2018). Ecological Response to Permafrost Thaw and

Consequences for Local and Global Ecosystem Services. *Annual Review of Ecology, Evolution, and Systematics*, *49*(279-301). https://doi.org/10.1146/annurev-ecolsys-121415-032349

Schuur, E. A. G., McGuire, A. D., Schädel, C., Grosse, G., Harden, J. W., Hayes, D. J., Hugelius, G., Koven, C. D., Kuhry, P., Lawrence, D. M., Natali, S. M., Olefeldt, D., Romanovsky, V. E., Schaefer, K., Turetsky, M. R., Treat, C. C., & Vonk, J. E. (2015). Climate change and the permafrost carbon feedback. *Nature*, *520*(7546), 171–179.

Seiler, C. (2019). *amber: Automated Model Benchmarking Package for the Canadian Land Surface Scheme*.

Seiler, C., Hutjes, R. W. A., Kruijt, B., & Hickler, T. (2015). The sensitivity of wet and dry tropical forests to climate change in Bolivia. *Journal of Geophysical Research. Biogeosciences*, *120*(3), 399–413.

Seiler, C., Hutjes, R. W. A., Kruijt, B., Quispe, J., Añez, S., Arora, V. K., Melton, J. R., Hickler, T., & Kabat, P. (2014). Modeling forest dynamics along climate gradients in Bolivia. *Journal of Geophysical Research. Biogeosciences*, *119*(5), 758–775.

Seiler, C., Melton, J. R., Arora, V. K., Sitch, S., Friedlingstein, P., Anthoni, P., Goll, D., Jain, A. K., Joetzjer, E., Lienert, S., Lombardozzi, D., Luyssaert, S., Nabel, J. E. M. S., Tian, H., Vuichard, N., Walker, A. P., Yuan, W., & Zaehle, S. (2022). Are terrestrial biosphere models fit for simulating the global land carbon sink? *Journal of Advances in Modeling Earth Systems*, *14*(5). https://doi.org/10.1029/2021ms002946

Seiler, C., Melton, J. R., Arora, V. K., & Wang, L. (2021). CLASSIC v1. 0: the open-source community successor to the Canadian Land Surface Scheme (CLASS) and the Canadian Terrestrial Ecosystem Model (CTEM)--Part 2: Global benchmarking. *Geoscientific Model*

Development, *14*(5), 2371–2417.

Shiga, Y. P., Michalak, A. M., Fang, Y., Schaefer, K., Andrews, A. E., Huntzinger, D. H., Schwalm, C. R., Thoning, K., & Wei, Y. (2018). Forests dominate the interannual variability of the North American carbon sink. *Environmental Research Letters: ERL [Web Site]*, *13*(8), 084015.

Smith, T. M., Shugart, H. H., Woodward, F. I., & Burton, P. J. (1993). Plant Functional Types. In A. M. Solomon & H. H. Shugart (Eds.), *Vegetation Dynamics & Global Change* (pp. 272–292). Springer US.

Sothe, C., Gonsamo, A., Arabian, J., Kurz, W. A., Finkelstein, S. A., & Snider, J. (2022). Large soil carbon storage in terrestrial ecosystems of Canada. *Global Biogeochemical Cycles*, *36*(2). https://doi.org/10.1029/2021gb007213

Strahler, Muller, Lucht, & Schaaf. (1999). MODIS BRDF/albedo product: algorithm theoretical basis document version 5.0. *Documentation and Information Services*. https://modis.gsfc.nasa.gov/data/atbd/atbd_mod09.pdf

Sulla-Menashe, D., Woodcock, C. E., & Friedl, M. A. (2018). Canadian boreal forest greening and browning trends: an analysis of biogeographic patterns and the relative roles of disturbance versus climate drivers. *Environmental Research Letters: ERL [Web Site]*, *13*(1), 014007.

Sulman, B. N., Salmon, V. G., Iversen, C. M., Breen, A. L., Yuan, F., & Thornton, P. E. (2021). Integrating arctic plant functional types in a land surface model using above- and belowground field observations. *Journal of Advances in Modeling Earth Systems*, *13*(4). https://doi.org/10.1029/2020ms002396

Takala, M., Luojus, K., Pulliainen, J., Derksen, C., Lemmetyinen, J., Kärnä, J.-P., Koskinen, J.,

& Bojkov, B. (2011). Estimating northern hemisphere snow water equivalent for climate research through assimilation of space-borne radiometer data and ground-based measurements. *Remote Sensing of Environment*, *115*(12), 3517–3529.

Tape, K., Sturm, M., & Racine, C. (2006). The evidence for shrub expansion in Northern Alaska and the Pan-Arctic. *Global Change Biology*, *12*(4), 686–702.

Teckentrup, L., De Kauwe, M. G., Pitman, A. J., Goll, D. S., Haverd, V., Jain, A. K., Joetzjer, E., Kato, E., Lienert, S., Lombardozzi, D., & Others. (2021). Assessing the representation of the Australian carbon cycle in global vegetation models. *Biogeosciences* , *18*(20), 5639–5668.

Tifafi, M., Guenet, B., & Hatté, C. (2018). Large differences in global and regional total soil carbon stock estimates based on SoilGrids, HWSD, and NCSCD: Intercomparison and evaluation based on field data from USA, England, wales, and France. *Global Biogeochemical Cycles*, *32*(1), 42–56.

Todd-Brown, K. E. O., Randerson, J. T., Post, W. M., Hoffman, F. M., Tarnocai, C., Schuur, E. A. G., & Allison, S. D. (2013). Causes of variation in soil carbon simulations from CMIP5 Earth system models and comparison with observations. *Biogeosciences* , *10*(3), 1717–1736.

UNFCCC. (2015). *Adoption of the Paris agreement, 21st conference of the parties*. United Nations Paris.

Ustin, S. L., & Gamon, J. A. (2010). Remote sensing of plant functional types. *The New Phytologist*, *186*(4), 795–816.

Verger, A., Baret, F., Weiss, M., Filella, I., & Peñuelas, J. (2015). GEOCLIM: A global climatology of LAI, FAPAR, and FCOVER from VEGETATION observations for 1999–

2010. *Remote Sensing of Environment*, *166*, 126–137.

Verger, A., Filella, I., Baret, F., & Peñuelas, J. (2016). Vegetation baseline phenology from kilometric global LAI satellite products. *Remote Sensing of Environment*, *178*, 1–14.

Verseghy, D. (2017). CLASS--The Canadian land surface scheme (v. 3.6. 2). *Climate Research Division, Science and Technology Branch, Environment Canada*, *35*.

Verseghy, D. L. (2000). The Canadian land surface scheme (CLASS): Its history and future. *Atmosphere-Ocean*, *38*(1), 1–13.

Verseghy, D. L. (2007). Class-A Canadian land surface scheme for GCMS. I. Soil model. *International Journal of Climatology*, *11*(2), 111–133.

Verseghy, D. L., McFarlane, N. A., & Lazare, M. (1993). Class—A Canadian land surface scheme for GCMS, II. Vegetation model and coupled runs. *International Journal of Climatology*, *13*(4), 347–370.

Walker, D. A., Raynolds, M. K., & Daniëls, F. J. A. (2005). The circumpolar Arctic vegetation map. *Of Vegetation …*. https://onlinelibrary.wiley.com/doi/abs/10.1111/j.1654-1103.2005.tb02365.x

Wang, A., Price, D. T., & Arora, V. (2006). Estimating changes in global vegetation cover (1850-2100) for use in climate models. *Global Biogeochemical Cycles*, *20*(3). https://doi.org/10.1029/2005gb002514

Wang, L., Bartlett, P., Arora, V. K., Chan, E., & Curasi, S. R. (2022). Mapping of ESA CCI land cover data to plant functional types for use in the CLASSIC land model. In *EGUsphere* (No. pp.1-43). https://doi.org/10.5194/egusphere-2022-923

Wang, L., Bartlett, P., Pouliot, D., Chan, E., Lamarche, C., Wulder, M. A., Defourny, P., & Brady, M. (2019). Comparison and Assessment of Regional and Global Land Cover

Datasets for Use in CLASS over Canada. *Remote Sensing*, *11*(19), 2286.

Wang, X., Jia, K., Liang, S., Li, Q., Wei, X., Yao, Y., Zhang, X., & Tu, Y. (2017). Estimating Fractional Vegetation Cover From Landsat-7 ETM+ Reflectance Data Based on a Coupled Radiative Transfer and Crop Growth Model. *IEEE Transactions on Geoscience and Remote Sensing: A Publication of the IEEE Geoscience and Remote Sensing Society*, *55*(10), 5539–5546.

Weber, M. G., & Flannigan, M. D. (1997). Canadian boreal forest ecosystem structure and function in a changing climate: impact on fire regimes. *Environmental Review*, *5*(3-4), 145–166.

White, J. C., Wulder, M. A., Hermosilla, T., Coops, N. C., & Hobart, G. W. (2017). A nationwide annual characterization of 25 years of forest disturbance and recovery for Canada using Landsat time series. *Remote Sensing of the Environment*, *194*, 303–321.

Wullschleger, S. D., Epstein, H. E., Box, E. O., Euskirchen, E. S., Goswami, S., Iversen, C. M., Kattge, J., Norby, R. J., van Bodegom, P. M., & Xu, X. (2014). Plant functional types in Earth system models: past experiences and future directions for application of dynamic vegetation models in high-latitude ecosystems. *Annals of Botany*, *114*(1), 1–16.

Wu, Verseghy, & Melton. (2016). Integrating peatlands into the coupled Canadian land surface scheme (CLASS) v3. 6 and the Canadian terrestrial ecosystem model (CTEM) v2. 0. *Geoscientific Model Development*. https://gmd.copernicus.org/articles/9/2639/2016/

Xiao, J., Ollinger, S. V., Frolking, S., Hurtt, G. C., Hollinger, D. Y., Davis, K. J., Pan, Y., Zhang, X., Deng, F., Chen, J., Baldocchi, D. D., Law, B. E., Arain, M. A., Desai, A. R., Richardson, A. D., Sun, G., Amiro, B., Margolis, H., Gu, L., … Suyker, A. E. (2014). Data-driven diagnostics of terrestrial carbon dynamics over North America. *Agricultural and*

Forest Meteorology, *197*, 142–157.

Xue, B.-L., Guo, Q., Hu, T., Wang, G., Wang, Y., Tao, S., Su, Y., Liu, J., & Zhao, X. (2017). Evaluation of modeled global vegetation carbon dynamics: Analysis based on global carbon flux and above-ground biomass data. *Ecological Modelling*, *355*, 84–96.

Zhang, T., Stackhouse, P. W., Gupta, S. K., Cox, S. J., Mikovitz, J. C., & Srb, N. G. (2011). *THE EFFECT OF CLOUD FRACTION ON THE RADIATIVE ENERGY BUDGET: The Satellite-Based GEWEX-SRB Data vs. the Ground-Based BSRN Measurements*. *2011*, A13B – 0261.

Zhang, Y., & Liang, S. (2020). Fusion of Multiple Gridded Biomass Datasets for Generating a Global Forest Aboveground Biomass Map. *Remote Sensing*, *12*(16), 2559.

Zhang, Y., Xiao, X., Wu, X., Zhou, S., Zhang, G., Qin, Y., & Dong, J. (2017). A global moderate resolution dataset of gross primary production of vegetation for 2000–2016. *Scientific Data*, *4*(1), 1–13.